ACS APPLIED NANO MATERIALS

Review

Magnetic-Nanosensor-Based Virus and Pathogen Detection Strategies before and during COVID-19

Kai Wu,* Renata Saha, Diqing Su, Venkatramana D. Krishna, Jinming Liu, Maxim C.-J. Cheeran,* and Jian-Ping Wang*

Cite This: ACS Appl. Nano Mater. 2020, 3, 9560−9580

Read Online

ACCESS | Metrics & More | Article Recommendations

ABSTRACT: The novel severe acute respiratory syndrome coronavirus 2 (SARS-CoV-2), which causes coronavirus disease 2019 (COVID-19), is a threat to the global healthcare system and economic security. As of July 2020, no specific drugs or vaccines are yet available for COVID-19; a fast and accurate diagnosis for SARS-CoV-2 is essential in slowing the spread of COVID-19 and for efficient implementation of control and containment strategies. Magnetic nanosensing is an emerging topic representing the frontiers of current biosensing and magnetic areas. The past decade has seen rapid growth in applying magnetic tools for biological and biomedical applications. Recent advances in magnetic nanomaterials and nanotechnologies have transformed current diagnostic methods to nanoscale and pushed the detection limit to early-stage disease diagnosis. Herein, this review covers the literature of magnetic nanosensors for virus and pathogen detection before COVID-19. We review popular magnetic nanosensing techniques including magnetoresistance, magnetic particle spectroscopy, and nuclear magnetic resonance. Magnetic point-of-care diagnostic kits are also reviewed aiming at developing plug-and-play diagnostics to manage the SARS-CoV-2 outbreak as well as preventing future epidemics. In addition, other platforms that use magnetic nanomaterials as auxiliary tools for enhanced pathogen and virus detection are also covered. The goal of this review is to inform the researchers of diagnostic and surveillance platforms for SARS-CoV-2 and their performances.

KEYWORDS: SARS-CoV-2, COVID-19, virus, magnetic nanosensor, biosensor, magnetoresistance, magnetic particle spectroscopy, nuclear magnetic resonance
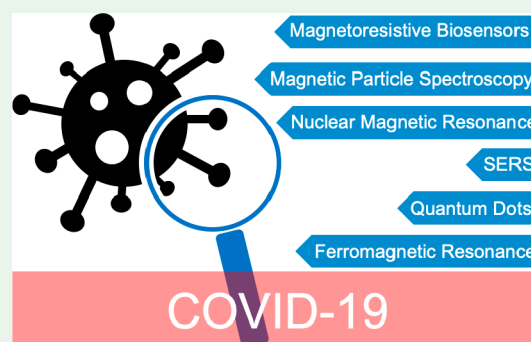
1. INTRODUCTION

In December 2019, a cluster of severe pneumonia cases was reported in Wuhan, Hubei Province, China.[1] Later, a novel strain of coronavirus belonging to the broad family of coronaviruses was subsequently isolated from bronchoalveolar lavage fluid.[2,3] The virus was initially named 2019 novel coronavirus (2019-nCoV) and later renamed severe acute respiratory syndrome coronavirus 2 (SARS-CoV-2).[4,5] The outbreak that began in China has rapidly expanded worldwide, and on January 30, 2020, the World Health Organization (WHO) declared the novel coronavirus infection a "Public Health Emergency of International Concern", and the illness was named coronavirus disease 2019 (COVID-19). COVID-19 was declared a pandemic by WHO on March 11, 2020, because of its rapid spread in various countries around the world. SARS-CoV-2 is an enveloped, positive-strand RNA virus with a large RNA genome of ∼30kb with genome characteristics similar to those of known coronaviruses.[6,7] The coronavirus genomic RNA encodes replication and transcription complexes from a single large open reading frame (ORF1ab) and structural proteins of the virus.[8] The major

structural proteins of coronavirus are spike (S), envelope (E), membrane (M), and nucleocapsid (N).

There is currently no medication to treat COVID-19. Because clinical manifestation of COVID-19 ranges from mild flulike symptoms to life-threatening pneumonia and acute respiratory illness, it is essential to have a proper diagnosis during an early stage of infection for efficient implementation of control measures to slow the spread of COVID-19.[9−11] Currently, real-time reverse-transcription polymerase chain reaction (RT-PCR) is the most widely used laboratory test for the diagnosis of COVID-19. RT-PCR detects SARS-CoV-2 RNA and targets different genomic regions of viral RNA.[12−14] Although RT-PCR is a sensitive technique, it requires expensive laboratory equipment and trained technicians to
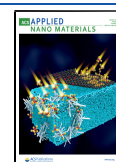
perform the test and can take up to 48 h to generate results. In addition, studies have found up to 30% false negative rate for RT-PCR in the early course of infection.[15−18] Several laboratories around the world are working on improving RT-PCR methods and developing alternative molecular diagnostic platforms. Isothermal nucleic acid amplification, which allows rapid amplification of target sequences at a single constant temperature, is employed in several tests including the ID NOW COVID-19 test from Abbott Diagnostics. ID NOW is a rapid, point-of-care (POC) test that allows the direct detection of viral RNA from the clinical sample without the need for RNA extraction. However, recent studies have found false negative rates ranging from 12 to 48% mainly because of inappropriate conditions of sample transportation and inappropriate samples.[19−21] Moreover, this can test only one sample per run. Recently, a rapid test for the detection of COVID-19 infection based on lateral-flow technology to detect viral nucleocapsid antigen has been developed by Abbott Diagnostics. Serological methods like enzyme-linked immunosorbent assay (ELISA) and lateral-flow immunochromatography, tests that detect antibodies, can be used to monitor immunity to infection and disease progression.[22] Although a negative SARS-CoV-2 antibody result does not rule out COVID-19, serological assays will help in assessing previous exposure to SARS-CoV-2 in a population and therefore have a potential use in understanding the epidemiology of COVID-19. Currently available serological assays can detect IgM, IgG, or IgA antibodies to spike (S) or nucleocapsid (N) protein.[23−25] However, potential cross-reactivity of SARS-CoV-2 antibodies with antibodies generated against other coronaviruses is a challenge in developing accurate serological tests for COVID-19.[26] Other nonmagnetic assay strategies for detecting SARS-CoV-2 have been extensively reviewed in ref 27−29 Recently, Liu et al. reviewed six promising methods including whole-genome sequencing, RT-PCR, nanopore target sequencing (NTS), antibody-based immunoassay techniques, paper-based biomolecular sensors, and clustered regularly interspaced short palindromic repeats Cas (CRISPR-Cas) system-based technology for the detection of SARS-CoV-2.[27] Whole-genome sequencing relies on identification of the whole sequence of the viral nucleic acid, which is the most comprehensive approach but is also expensive and time-consuming. RT-PCR first reverse-transcripts the viral RNA into complementary DNA sequences, followed by the exponential amplification of gene fragments with the help of target-specific primers. NTS technology combines the advantages of whole-genome sequencing and RT-PCR. The target gene sequence first is amplified and then goes through a sequencing process, where both the concentration of analytes and detailed nucleic acid sequence information can be analyzed. The CRISPER-Cas method makes use of the special mechanism of CRISPER RNAs and Cas13a. Cas13a, which is reprogrammed with CRISPER RNAs, can be activated after recognition of the target RNA, leading to cleavage of a reporter RNA that is bound to a fluorescent quencher. Paper-based biomolecular sensors have also been developed based on the programmable RNAs. Upon exposure to a trigger RNA, the hairpin within the sensor begins to unwind, which exposes the ribosomal binding sites and enables downstream protein translation. Besides the RNA-based technologies, antibody-based immunoassay, which relies on the specific reaction between the antibodies and target antigens, is also promising for the rapid detection of SARS-CoV-2. The development of

high-quality antibodies as well as the improvement of the testing sensitivity and specificity is the key to the large-scale application of these technologies. Although RT-PCR is the most-widely employed approach, the antibody-based immunoassay techniques, paper-based biomolecular sensors, and CRISPR-Cas system-based methods are expected to be further developed into large-scale screening methods in the future. On the other hand, NTS, with high sensitivity, comprehensiveness, and low cost, could be the most suitable method for the rapid detection of suspected viral infection that cannot be diagnosed effectively by other methods. In June 2020, Wang et al. reported the NTS-based detection of SARS-CoV-2 and other respiratory viruses simultaneously within 6−10 h, with a limit of detection (LOD) of 10 standard plasmid copies per reaction.[30] The specificity of this NTS for SARS-CoV-2 reaches 100%. It can effectively monitor muted nucleic acid sequences, categorize types of SARS-CoV-2, and detect other respiratory viruses from samples. In addition to the technologies mentioned above, Shan et al. reported a nanomaterial-based sensor array with the ability to detect SARS-CoV-2 from exhaled breath.[31] The sensor is composed of organic film elements and inorganic nanomaterials. The organic film elements are linked to gold nanoparticles and function as the sensing layer, which either swells or shrinks upon exposure to volatile organic compounds, leading to a change in the device resistance. The sensor was used in the clinical study with 94% and 76% accuracy in discriminating between the patients and the controls for training and test set data, respectively. The discrimination between COVID-19 patients and patients with other lung infections was also demonstrated with accuracies of 90% and 95% for training and test set data, respectively.

Among other biosensing technologies, magnetic biosensors have attracted special attention in the past 20 years. Both surface- and volume-based magnetic biosensors have been developed for the detection of viruses, pathogens, cancer biomarkers, metallic ions, etc.[32−42] In magnetic biosensors, the magnetic tags [usually magnetic nanoparticles (MNPs)] are functionalized with antibodies or DNA/RNA probes that can specifically bind to target analytes.[43−45] The concentration of target analytes is thus converted to the magnetic signals that are generated by these magnetic tags. Compared to optical, plasmonic, and electrochemical biosensors, magnetic biosensors exhibit low background noise because most of the biological environment is nonmagnetic. The sensor signal is also less influenced by the type of sample matrix, enabling accurate and reliable detection processes.[46] The number of published papers on magnetic biosensors is summarized in Figure 1, which indicates an increasing scientific interest in this topic.

Most magnetic biosensors fall into several categories, namely, magnetoresistance (MR) sensors, magnetic particle spectroscopy (MPS) platforms, and nuclear magnetic resonance (NMR) platforms. MR sensors are surface-based technologies that are sensitive to the stray field from the MNPs bound to the proximity of the sensor surface. MR-based magnetic bioassays are reviewed in section 2, and this kind of assay scheme is achieved by converting the binding events of MNPs (due to the presence of target analytes) to readable electric signals. The sensitivity of MR bioassays largely depends on the magnetic properties of the magnetic stacks in the MR sensors as well as MNPs. Optimization of the thin-film structures in MR sensors is needed to acquire magnetic field
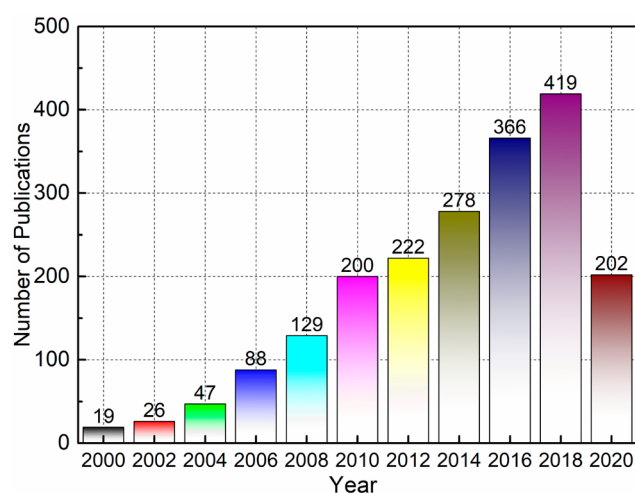
Figure 1. Number of publications on magnetic biosensors in the past 20 years as of July 8th, 2020. The data were acquired from the Web of Science core collection with the keywords "magnetic biosensors" and "magnetic biological sensors".

response with high sensitivity and linearity. In the meantime, MNPs employed in the immunoassays are required to exhibit high magnetic moments while maintaining the superparamagnetic state. On the contrary, MPS platforms are volume-based technologies that (reviewed in section 3) directly detect the dynamic magnetic responses of MNPs; thus, MNPs are the only signal sources and indicators for probing target analytes from nonmagnetic media. Consequently, the magnetic properties of MNPs such as saturation magnetization and anisotropy are the key parameters for optimization of the device performance. Other factors such as the electrical and magnetic properties of the excitation and pick-up coils also need to be considered. NMR platforms (reviewed in section 4) use MNPs as contrast enhancers to introduce local magnetic field inhomogeneity and to disturb the precession frequency

variations in millions of surrounding water protons. Thus, high-sensitivity NMR-based bioassays intrinsically benefit from the MNP contrast agents. In addition to the desired magnetic properties for MR and MPS platforms, MNPs in NMR systems are also required to exhibit high transverse relaxivity. Different magnetic nanosensor-based platforms for virus and pathogen detection are reviewed, and comparisons are made in Table 1. Other bioassay platforms that use magnetic nanomaterials as auxiliary tools to enhance the detection performances are also reviewed in section 5. In this review, magnetic biosensor application in virus and pathogen detection will be summarized and discussed based on the different working principles of the technologies.

2. MR PLATFORMS

2.1. MR. MR was first discovered by William Thompson, who coined the term anisotropic magnetoresistance (AMR).[47] The physical observation of AMR shows that the resistivities of both Ni and Fe increase when the charge current is applied parallel to the magnetization and decrease when the charge current is applied perpendicular to the magnetization.[48] This AMR effect originates from the spin−orbit interactions and was experimentally and quantitatively demonstrated by Fert and Campbell.[49] However, the maximum resistance change recorded from AMR devices is only around 2%, which renders it unsuitable for most applications. Regarding this, a detailed review of the AMR effect in thin films and bulk materials can be found in ref 48. Herein, the AMR biosensors will not be discussed due to their limited applications in magnetic biosensing.

Giant magnetoresistance (GMR) was at first observed from the Fe/Cr multilayers grown with molecular-beam epitaxy by Albert Fert and Peter Grunberg.[50,51] These multilayers exhibit a resistance change significantly higher than that of the AMR devices. The GMR effect primarily exists in multilayer structures with alternating ferromagnetic and nonmagnetic metallic layers. When the magnetizations of two adjacent

Table 1. Comparison of Different Magnetic Nanosensors

| platform	assay time	pathogen	LOD	evaluated matrix	ref
GMR	<10 min	H1N1	15 ng/mL (0.26 nM) for H1N1 nucleoprotein	PBS[a]	73
		H3N2v	125 $TCID_{50}$/mL		
	<10 min	H1N1	250 $TCID_{50}$/mL	nasal swab	72
		H3N2v	250 $TCID_{50}$/mL		
	15 min	HBV	200 IU/mL DNA	serum	75
	N.A.	E. coli O157H:H7	100 CFU/mL antigen in a 1 mL sample	PBS	77
	N.A.	M. tuberculosis	1 pM ESAT-6 protein	N.A.	78
MTJ	100 min	HEV	N.A.	PBS	83
		L. monocytogenes	N.A.		
	N.A.	HIV	0.01 μg/mL (4.16 nM) antigen p24	N.A.	84
MPS	30 min	C. botulinum	0.22, 0.11, and 0.32 ng/mL (1.46, 0.7, and 2.2 pM) for BoNT-A, -B, and -E, respectively	milk, apple, and orange juices	85
	25 min	S. aureus	4 and 10 pg/mL (0.18 and 0.34 pM) for TSST and SEA	milk	86
	2 h		0.1 and 0.3 ng/mL (4.5 and 10.3 pM) for TSST and SEA		
	10 s	H1N1	4.4 pmol for H1N1 nucleoprotein	PBS	87
	42 min	SARS-CoV-2	2.96 ng/mL (19.7 pM) for SARS-CoV-2 antispike−protein antibodies	PBS	88
			3.36 ng/mL (22.4 pM) SARS-CoV-2 antispike−protein antibodies	serum	
NMR	1 min	E. coli O157:H7	76 CFU/mL	water	89
			92 CFU/mL	milk	
	2.5 h	M. tuberculosis	1 nM ssDNA in 1 μL sample	sputum	90

[a]PBS: phosphate-buffered saline.
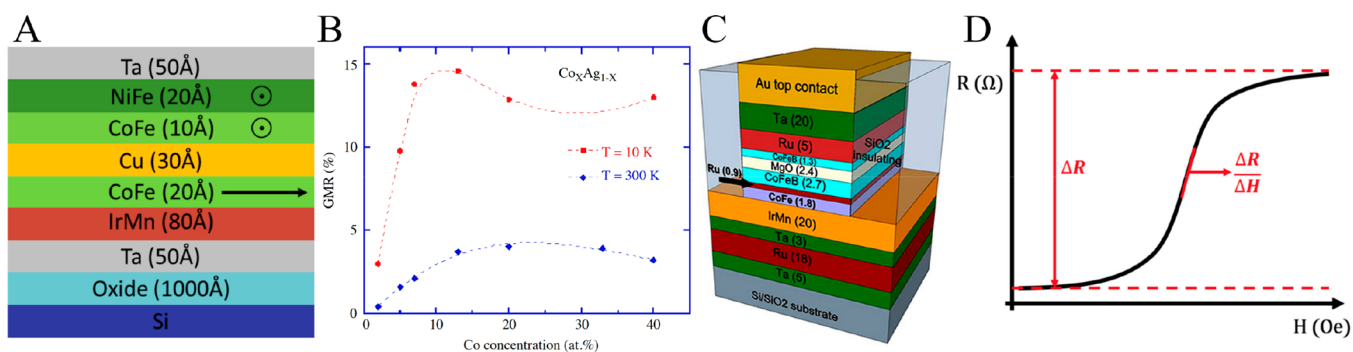
Figure 2. (A) Typical GMR stack structure used for biosensing. (B) MR of the Co−Ag matrix, the evidence of granular GMR. (C) Typical MTJ structure used for biosensing. (D) Typical transfer curve of a MR sensor. Part A was reproduced with permission from ref 68. Copyright 2019 IOP Publishing. Part B was reproduced with permission from ref 56. Copyright 2006 Elsevier. The image in part C adapted from ref69 is licensed under CC BY-ND 2.0. The image in part D adapted from ref 70 is licensed under CC BY-ND 2.0.
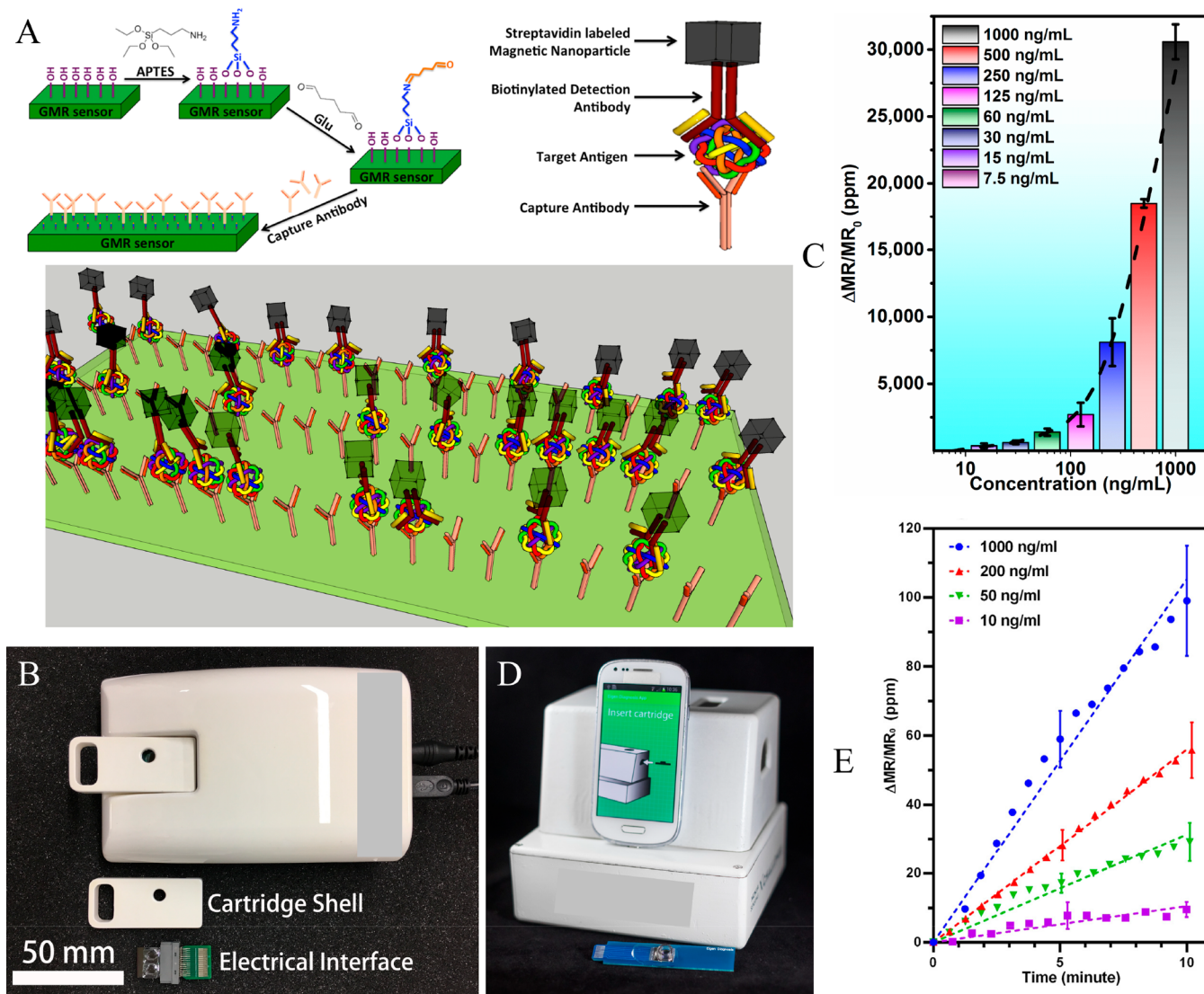

Figure 3. (A) Sandwich immunoassay mechanism of a GMR biosensor forming a capture antibody−target antigen−detection antibody−MNP complex. (B) Photograph of the GMR-based hand-held device reported by researchers from University of Minnesota. (C) Response curves of H1N1 nucleoprotein as detected by the hand-held device in part B showing a LOD of 15 ng/mL. (D) Photograph of another GMR-based portable device reported by the researchers from Stanford University. (E) Response curves of IgG antibodies detected by the device shown in part D depicting a LOD of 10 ng/mL. The image in part A adapted from ref 72 is licensed under CC BY-ND 2.0. Parts B and C were reproduced from ref 73. Copyright 2017 American Chemical Society. Parts D and E were reproduced with permission from ref 74. Copyright 2016 Elsevier.

ferromagnetic layers are parallel, the multilayers show low resistance, and when the magnetizations are antiparallel, the multilayers exhibit a high-resistance state. The industrial breakthrough for GMR discovery was made when Parkin et al. observed the GMR effect from direct-current-sputtered multilayer structures.[52] Although the GMR effect was primarily observed in a thin film or layered system (Figure 2A), it is also observed in other systems such as Co−Au, Co−Ag, and Fe− Ag granular films.[53−57] The GMR effect in granular films (Figure 2B) is highly related to the spin-dependent interfacial scattering, interparticle coupling, and several are significant for biosensing purposes because of their ability to adapt to the shapes of different biomolecules.[58,59] In comparison to other types of sensors, the ability of flexible GMR sensors to respond to an external magnetic field makes them a perfect candidate for wearable real-time body activity monitoring and evaluation of drug-delivery effectiveness. Because no experimental demonstration on the flexible MR-based detection of viruses/pathogens has been reported, further discussion on flexible GMR-based biodetection is restricted in the subsequent sections.

Magnetic tunnel junctions (MTJs) have stack structures (Figure 2C) similar to that of the GMR spin valves except that the adjacent ferromagnetic layers are separated by an insulating layer, which is usually an oxide. In the earlier days, AlO_x was used.[60,61] Later, this insulating layer was replaced by a MgO material for smaller lattice mismatch and interface instability and, thus, higher tunnel magnetoresistance (TMR) ratio.[62,63] The most important characteristic of a MTJ structure is its transfer curve, as shown in Figure 2D. In the transfer curve, two characteristics are of utmost importance: the MR ratio and sensitivity. The physical characterization of the MR ratio is the rate of change in the MR device resistance along with varying magnetic field. Its sensitivity is measured by the slope of the transfer curve at an intensity of the magnetic field. In this regard, an interesting point to note is the trade-off between the sensitivity and linear magnetic field response range for MR sensors. A large linear response range in the transfer curve is attained with great ease in GMR sensors, although this comes with a compromise on the sensitivity. On the other hand, even though MTJ sensors possess high sensitivity, additional stack designs or supporting parts such as bias magnets are required to achieve high linearity.[64−66] Another factor that comes into play for all sensors in the nanoscale is the signal-to-noise ratio (SNR). Generally, MTJ sensors show higher SNR than GMR sensors. However, the shot noise from the conduction medium can cause the SNRs of MTJs to suffer.[67] With the advancing of thin-film deposition and nanofabrication technologies, the TMR ratio has increased dramatically during the past 20 years from ∼20% to over 200%.[62,68−70]

2.2. GMR Platform. Since Baselt et al. reported the first GMR-based biosensor using the Bead Array Counter microarray, GMR-based biosensing has been attracting increasing attention among the community.[71] This section reviews the GMR biosensors for detecting viruses and pathogens and compares their LODs and advantages over the existing biosensing tools. Take the sandwich immunoassay as an example (Figure 3A), where the capture antibodies specifically targeting analytes (such as antigens from viruses/pathogens) are prefunctionalized on the GMR sensor surface. Then biofluid samples are added, and specific antibody−antigen bindings take place on the sensor surface. Usually a washing step is added to remove the unbound analytes from the sensing

areas. Then the detection-antibody-functionalized MNPs are added to the GMR sensing areas, forming the MNP−detection antibody−antigen−capture antibody complexes. Thus, the amount of MNPs captured to the proximity of the sensor surface is directly proportional to the number of antigens in the testing sample. Furthermore, this sandwich immunoassay scheme significantly enhances the detection specificity. To attain the best performance, superparamagnetic MNPs (SPMNPs) are prevalently used to avoid clustering and sedimentation to the sensor surfaces. There are several factors to be considered for MNP-based magnetic immunoassays. First, the size of the MNPs should stay under the critical size of a single-domain-to-multidomain transition, which is around 25 nm for iron oxide MNPs, to maintain the superparamagnetic state. Second, the saturation magnetization increases with the particle size until it reaches the bulk value. As a result, the size of the MNPs should be increased to acquire high saturation magnetization but also be small enough to stay in the single-domain state. Third, the uniformity of both the sizes and shapes of MNPs is important in a detection process with high repeatability. Because the signals of the magnetic sensors depend on the stray field from MNPs, poor uniformity will lead to signal variation from each binding event between the target analyte and sensor surface, thus resulting in different signal levels for multiple measurements of target analytes with the same concentration.

Krishna et al. reported a GMR benchtop system for detection of the H1N1 strain of the influenza A virus (IAV) within a concentration range of $10^3–10^5$ $TCID_{50}$/mL.[72] Wu et al. reported a portable GMR biosensing device named Z-Lab (Figure 3B) to detect IAV.[73] They achieved a LOD of 15 ng/ mL for detecting H1N1 nucleoprotein (Figure 3C) and a LOD of 125 $TCID_{50}$/mL for detecting purified H3N2 variant virus (H3N2v) from buffer solutions, with an overall assay time of less than 10 min. Later, Su et al. reported the wash-free immunoassay scheme for detecting H1N1 and H3N2v from spiked nasal-swab samples with a reported LOD of 250 $TCID_{50}$/mL.[32] This wash-free immunoassay approach allows for detections handled by nontechnicians with minimum training requirements. Another group from Stanford University reported a similar GMR-based portable system for on-site bioassays (Figure 3D). They reported the multiplexed assay of human immunoglobulin G and M (IgG and IgM) antibodies with sensitivities down to 0.07 and 0.33 nM, respectively. Figure 3E shows the real-time signals as measured by their portable device for detecting various concentrations of IgG over a 10 min measurement period.[74] Zhi et al. reported the detection of Hepatitis B virus (HBV) using a GMR biochip integrated with a microfluidic channel with a detection sensitivity of 200 IU/mL for HBV DNA molecules.[75] In their work, the integration of a microfluidic channel increased the ease of handling smaller sample volumes on the sensing area. A good follow-up of this work with significantly improved LODs down to 10 copies of target HBV DNA molecules has been reported.[76] GMR platforms have also been reported for bacteria detection. For instance, Sun et al. reported the detection of *Escherichia coli O157H:H7* antigen using the GMR biosensing scheme with a reported LOD of 100 colony-forming units (CFU)/mL.[77] Gupta et al. reported the detection of *Mycobacterium tuberculosis* specific antigen− ESAT-6 using the GMR scheme and a LOD of 1 pM.[78]

The key takeaway point here is that several experimental demonstrations of magnetic assays for virus detection based on
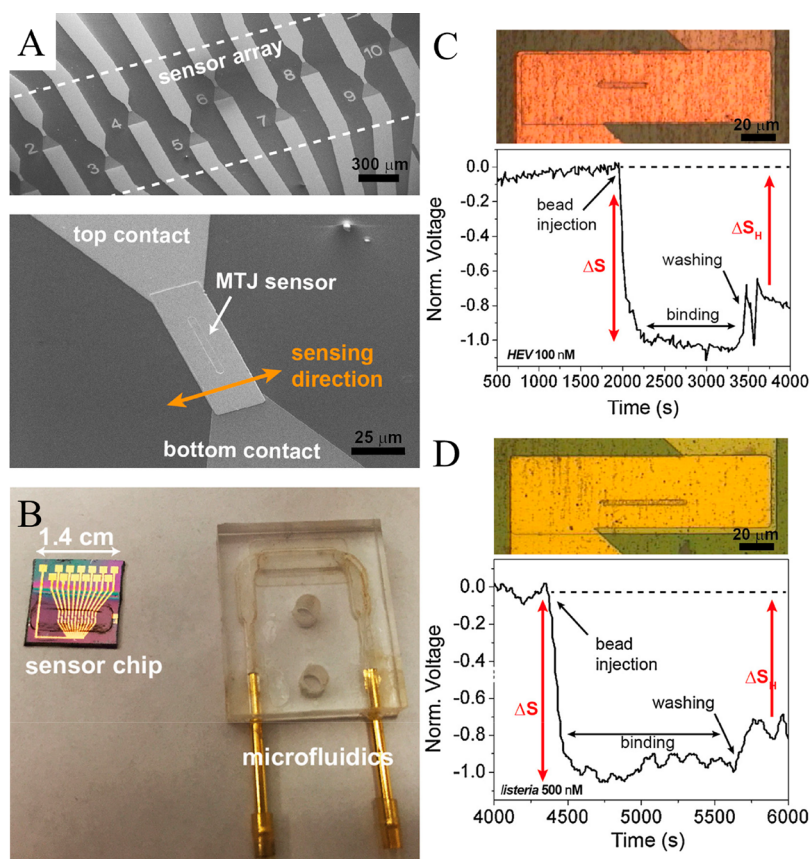
Figure 4. (A) SEM image of the 12 MTJ sensors array. (B) Photograph of the microfluidic channel integrated with the MTJ biosensors to facilitate the handling of extremely small sample volumes. Normalized MTJ signals from sensors functionalized with (C) HEV DNA probes for detecting 100 nM HEV target DNA and (D) Listeria DNA probes for detecting 500 nM Listeria target DNA. Top panels show the photographs of sensor areas after magnetic bead immobilization. Reproduced with permission from ref 83. Copyright 2017 Elsevier.

GMRs, and the reported LODs indicate that GMR-based bioassay is one of the promising candidates for the on-site, rapid, and sensitive detection of COVID-19.

2.3. MTJ Platform. The first-ever proof-of-concept MTJ as a biosensor was reported by Grancharov et al. in 2005.[79] They demonstrated a unique method for antigen and DNA detection at room temperature using monodispersed manganese ferrite nanoparticles as the magnetic tags. Since then, there have been several attempts to employ MTJs as biosensors.[70,80−82] However, most of their attempts were limited to genotyping applications of TMR sensors. In the year of 2017, Sharma et al. demonstrated a poly(methyl methacrylate) microfluidic integrated MTJ platform (Figure 4A,B) for detecting pathogenic DNA from Hepatitis E virus (HEV), *Listeria monocytogenes*, and *Salmonella typhimurium* bacteria.[83] Parts C and D of Figure 4 show that the normalized signal acquires as a function of time from MTJ sensors functionalized with HEV and Listeria target DNA probes, respectively, with an assay time of around 100 min. The excellent sensitivity and specificity of the microfluidic integrated MTJ platform could pave the way for a lab-on-chip multiplexed apparatus and the POC detection of pathogenic antigens. Very recently, Li et al. experimentally demonstrated the detection of HIV-1 antigen p24 by MTJ sensors with an assay time of less than 10 min and a LOD on the order of 0.01 μg/mL.[84]

With improved circuitry design and the ease of nanofabrication, there is a trend to use MTJ sensors for bioassays. Gervasoni et al. used a 12-channel dual lock-in platform to improve the circuitry for signal generation and acquisition in their MTJ sensing system.[82] They achieved a sub-ppm resolution of the lock-in amplifier and an order of magnitude better than a commercial state-of-the-art instrument. However, there are several disadvantages of MTJs as biosensors compared to GMR sensors. The requirement for top electrodes increases the distance between the MNPs bound to the surface and the free layer of the MTJ sensor. Because the stray fields of the MNPs decay rapidly with an increase of the distance, the sensitivity of the MTJ sensors is often sacrificed despite their high TMR ratio. Furthermore, the difficulty to achieve high linearity and low coercivity also remains a challenge for MTJs. More dedicated designs of the stack structure and the fabrication process are needed to take full advantage of the high signal level induced by the large TMR ratio.

3. MPS PLATFORMS

3.1. MPS. MPS was first reported by Nikitin et al. and Krause et al. in 2006.[91,92] It is a derivative technology from magnetic particle imaging (MPI), where the tomographic images can be reconstructed by exploiting the nonlinear magnetic responses of MNPs.[93,94] Herein, in MPS-based immunoassays, the nonlinear magnetic responses of MNPs along with their rotational degree of freedom are used as metrics for different biosensing purposes.[44] In a MPS platform, external sinusoidal magnetic fields (also called excitation fields) are applied to periodically magnetize (and magnetically
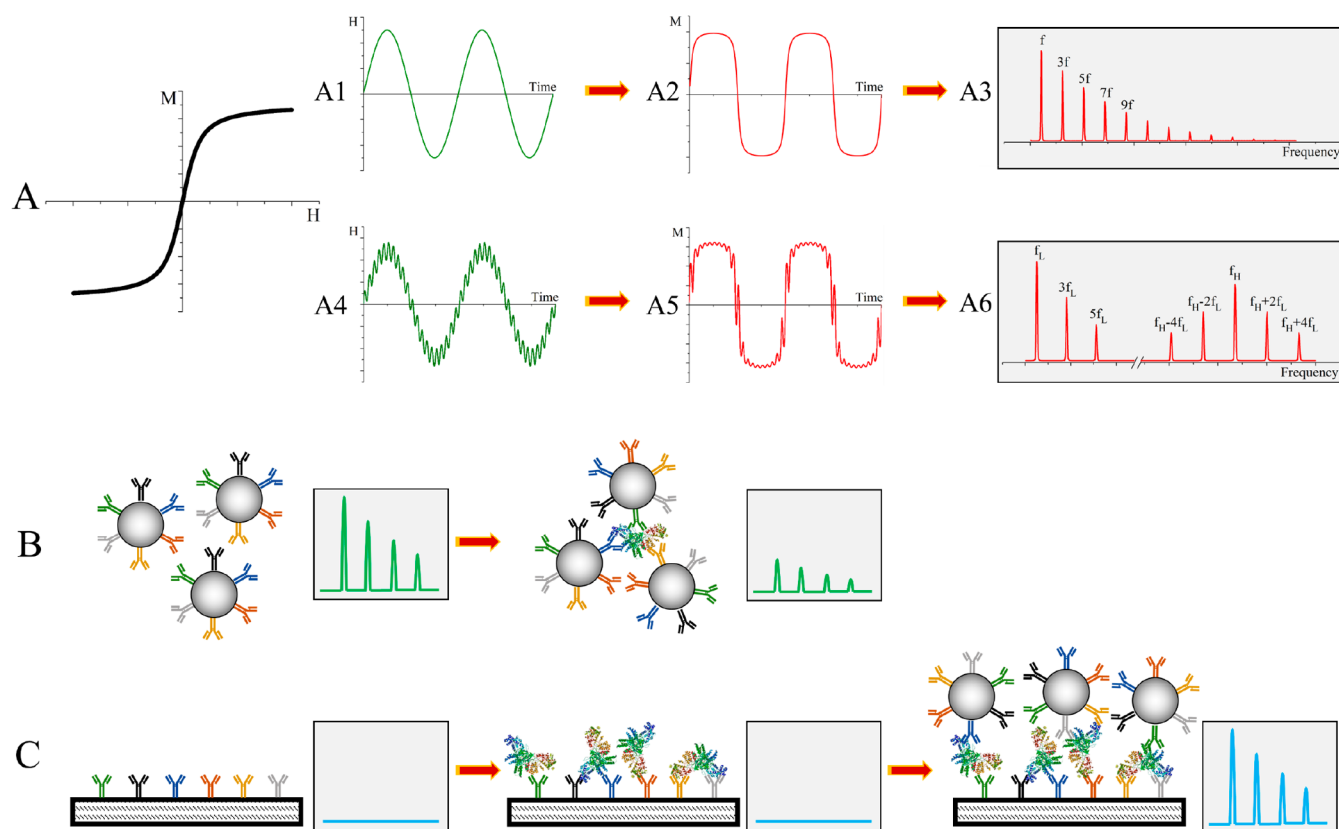
Figure 5. (A) Nonlinear magnetic responses of MNPs. A1−A3 and A4−A6 are the monofrequency and dual-frequency modes, respectively. A1 and A4 are the time-domain excitation fields. A2 and A5 are the time-domain magnetic responses. A3 and A6 are the MPS spectra extracted from the pick-up coils. (B) Schematic drawing of the volume-based MPS immunoassay. (C) Schematic drawing of the surface-based MPS immunoassay.

saturate) the MNPs, as shown in Figure 5A1,A3.[85−87,95−101] The time-varying dipolar magnetic fields generated by MNPs as a response to the applied fields (Figure 5A2,A4) are monitored by pick-up coils. As a result of Faraday's law of induction, the time-varying electric voltages from pick-up coils are recorded and MPS spectra are extracted for analysis, as shown in Figure 5A3,A6). Nowadays, there are two excitation field modes of MPS platforms that have been frequently reported: the monofrequency and dual-frequency modes. In a monofrequency MPS platform, one sinusoidal magnetic field with frequency f is applied and higher odd harmonics at $3f$ (the third harmonic), $5f$ (the fifth harmonic), $7f$ (the seventh harmonic), etc., are observed because of the nonlinear magnetic responses of MNPs.[95,96,102] On the other hand, in a dual-frequency MPS platform, two sinusoidal magnetic fields with frequencies f_H and f_L are applied. The low-frequency field f_L periodically magnetizes MNPs, while the high-frequency field f_H modulates these higher odd harmonics to the high-frequency range. Thus, higher odd harmonics at $f_H \pm 2f_L$ (the third harmonics), $f_H \pm 4f_L$ (the fifth harmonics), $f_H \pm 6f_L$ (the seventh harmonics), etc., are observed.[97,99,103−106] Although different in excitation modes, the detection mechanisms periodically magnetize the MNPs, and the extractions of higher odd harmonics as a result of nonlinear magnetic responses are identical.

In addition, there are two types of MPS-based immunoassay platforms: volume- and surface-based platforms (Figure 5B,C). Although both platforms use dynamic magnetic responses of MNPs for characterization, the degrees of freedom are different. In volume-based MPS platforms, MNPs are dispersed

in the liquid phase. Upon the application of external magnetic fields, their magnetic moments relax to align to the external fields through the joint Brownian and Néel relaxation processes, where Brownian relaxation is the physical rotation of a whole MNP with its fixed magnetic moment and Néel relaxation is the rotation of the magnetic moment inside a stationary MNP. For volume-based MPS platforms, single-core, SPMNPs that realign magnetic moments to external fields through a Brownian-relaxation-dominated process are favored. The Brownian relaxation process is affected by the liquid viscosity, hydrodynamic volume of MNP, and temperature (note: other factors such as the magnetic field amplitude, dipolar interactions between neighboring MNPs, magnetic properties of MNPs such as saturation magnetization, anisotropy, etc., are not in the scope of this review).[105−111] By surface functioning MNPs with biological/chemical reagents such as antibodies, DNA, RNA, and proteins, the MNPs serve as high-specificity probes to capture target analytes from biofluid samples. As shown in Figure 5B, the successful recognition and binding events on MNPs cause increased hydrodynamic volume. Thus, Brownian relaxation is inhibited but is still the dominant relaxation mechanism, and magnetic responses are weakened. Larger phase lags between the magnetic moments and external fields are detected, and lower harmonic amplitudes are observed from the MPS spectra. In this volume-based MPS platform, immunoassay is achieved by monitoring the reduced rotational freedom of MNPs in the testing suspension. On the other hand, in the surface-based MPS platform, surface-functionalized MNPs are captured to a solid substrate (i.e., reaction surface) and their
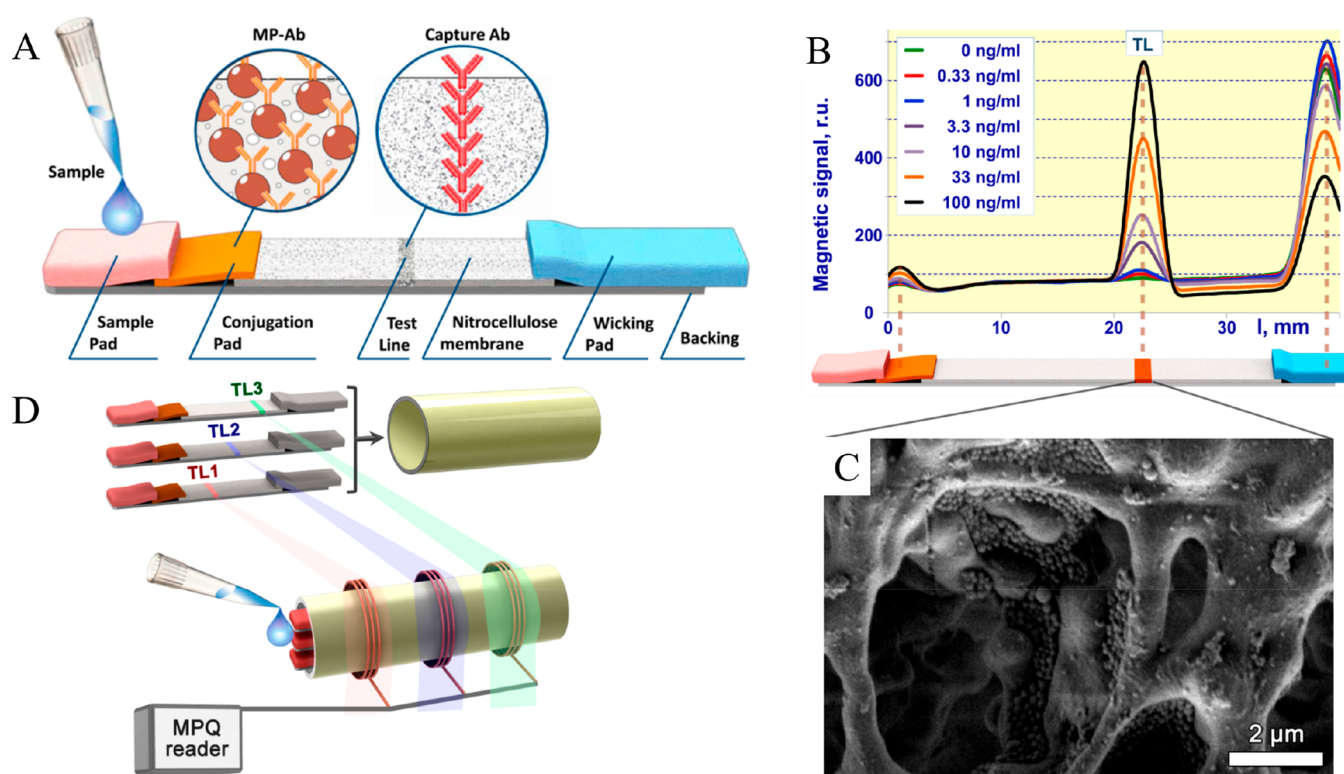
Figure 6. (A) Test-strip design based on sandwich-lateral-flow assay. (B) Distributions of MNPs along the lateral-flow test strip for different concentrations of BoNT-A. (C) SEM image of MNPs specifically captured on the membrane. (D) Multiplexed assay setup: several single-plex test strips with dissimilar positions of the test lines are combined in a miniature cartridge. The cartridge with a sample deposited onto its front end is inserted into the portable MPQ reader (i.e., MPS). Reproduced from ref 85. Copyright 2016 American Chemical Society.

Brownian rotational freedom is inhibited or blocked for different scenarios, as shown in Figure 5C. As a result, immunoassays are achieved by "counting" the number of MNPs captured to the solid substrate.

3.2. Surface-Based MPS Platform. Orlov et al. reported a multiplexed lateral-flow (LF) assay for the detection of botulinum neurotoxin (BoNT) types A, B, and E.[85] BoNT-A, -B, and -E are proteins produced by anaerobic bacteria of *Clostridium botulinum* widely present in soil and water. In their work, multiplexing is realized by combining the MPS platform with lateral-flow measurement. The lateral-flow method is based on various optical labels such as latex, Au, Ag, and QDs, with this method alone, it is difficult to achieve high-sensitivity, quantitative immunoassays, especially in opaque media.[112−116] By replacement of these optical labels with magnetic labels (i.e., MNPs), a potentially high-sensitivity, high-stability, and low-background-noise biosensing platform is achieved. Herein, the authors combined three test strips in a cartridge. Each test strip is named A-strip, B-strip, and E-strip, respectively, for the intended detection of BoNT-A, -B, and -E, respectively, as shown in Figure 6D. Each strip is composed of overlapping sample pad, conjugation pad, nitrocellulose, and wicking pad on an adhesive plastic backing sheet, as shown in Figure 6A. The anti-BoNT capture antibodies (labeled as capture Ab in the figure) are deposited onto the nitrocellulose membrane labeled as test line. The corresponding MNP−detection antibody complexes (labeled as MP-Ab in the figure) are deposited on the conjugation pad. During an assay process, the testing sample is deposited onto the sample pad and the fluid migrates along the test strip under capillary action. The target analytes bind to MP-Ab and capture Ab on the test line. As

shown in Figure 6B, the distributions of MNPs along the test strip exhibit three peaks corresponding to the remaining MNPs left on the conjugation pad, MNPs bind on the test line because of the presence of target analytes, and unbound MNPs collected on the wicking pad. The magnetic signal amplitudes recorded by MPS [labeled as the magnetic particle quantification (MPQ) reader in the figure] are positively correlated with the concentration (quantity) of target analytes. The specifically captured MNPs on the test line of the nitrocellulose membrane can be seen in the scanning electron microscopy (SEM) image shown in Figure 6C. The multiplexed assay procedures and measuring setup are like the single-plex assay, by replacing the single-plex strip with a cartridge. The sample is deposited on the cartridge, and after ~25 min, the cartridge is inserted into the MPQ reader for measurements. Using this method, the authors have successfully and simultaneously detected three botulinum toxin stereotypes from complex liquid matrixes such as whole milk and juices.

The authors successfully combined the MPS method with the lateral-flow method. By the conjugation of different capture antibodies onto different locations of a test strip, a multiplexed assay platform is achieved. By replacement of the optical labels with MNPs, the measurements can analyze media regardless of the optical properties, offering sensitivities on the level of laboratory-based quantitative methods.

Orlov et al. reported the application of the MPS platform for the detection of toxins produced by *Staphylococcus aureus*.[86] These toxins are widely present in the environment and the cause of diverse fatal illnesses such as severe gastrointestinal diseases and toxic shock. In their work, they introduced a novel
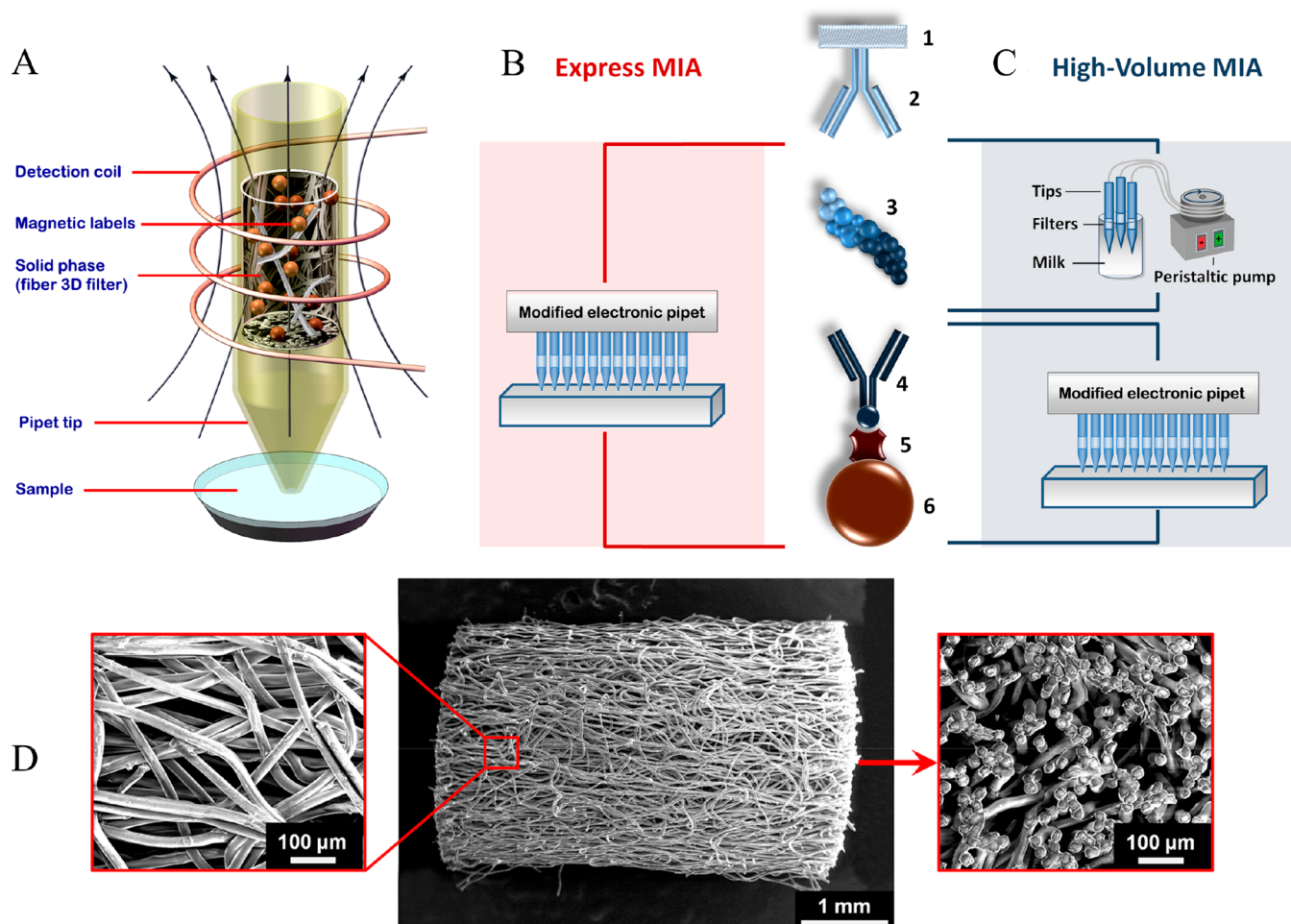
Figure 7. (A) Schematic drawing of 3D porous filters as a solid-phase immunoassay substrate in a cylinder. Schematic drawings of a sandwich-structure magnetic immunoassay on 3D fiber filters: (B) express MIA setup; (C) high-volume MIA setup. (D) SEM image of cylindrical 3D fiber filters. Reproduced from ref 86. Copyright 2012 American Chemical Society.

magnetic immunoassay on the 3D fiber solid phase (Figure 7D) that fits into a standard automatic pipet tip, as shown in Figure 7A. The 3D porous filter surfaces are immobilized with capture antibodies specific to a definite toxin. These as-prepared solid-phase filter immobilized with antibodies can be stored for a long time without compromising the properties. Two measurement formats are proposed: one for analysis of the small-volume samples (Figure 7B, labeled as express MIA) and the other for analysis of the large-volume samples (Figure 7C, labeled as high-volume MIA). In the express MIA, samples are dispensed simultaneously through all of the tips by an electronic pipet. In the high-volume MIA, the testing sample is pumped through the 3D fiber filters and the sample volume is determined by the pumping rate and time. In this step, the target analytes flowing through 3D porous filters are captured by the capture antibodies from the solid-phase filter. Further steps are the same for both formats. After the samples are passed through the filters, each filter is washed to removed unbound reagents. Then 7 min of dispensing of the detection antibody−MNP complexes is carried out followed by another cycle of the washing step. The MNPs that bind to the immunocomplex on the 3D porous fiber surfaces serve as labels to be recorded by the MPS reader.

In June 2020, Pietschmann et al. reported the portable MPS surface-based immunoassay platform MInD (magnetic im-munodetection) for the detection of SARS-CoV-2-specific antibodies.[88] In their work, a porous polyethylene filter matrix coated with a SARS-CoV-2 spike−protein peptide is serving as the reaction surface (called immunofiltration columns in the paper). Varying concentrations of SARS-CoV-2 antispike−protein antibodies in phosphate-buffered saline (PBS) and human serum samples are spiked through the surface, followed by a washing step to remove unbound antibodies. Then biotinylated secondary antibodies are added, followed by another washing step. Finally, streptavidin-coated MNPs are added to the reaction surface, forming a [SARS-CoV-2 spike−protein peptide]−[SARS-CoV-2 antispike−protein anti-body]−[secondary antibody]−[MNP] structure. After a final washing step, the MPS spectra of captured MNPs are measured. They achieved LODs of 2.96 and 3.36 ng/mL for the detection of SARS-CoV-2 antispike−protein antibodies from PBS and human serum, respectively. It shows better sensitivity and a wider detection range than the commonly used analytical biochemistry assay ELISA. However, negative control groups are PBS and serum without antispike−protein antibodies. The detection of antibodies can provide a larger window of time for the indirect detection of SARS-CoV-2 because antibodies are generated in response to the infection. Antibody testing is very useful for the surveillance of COVID-19. One potential challenge of developing accurate antibody
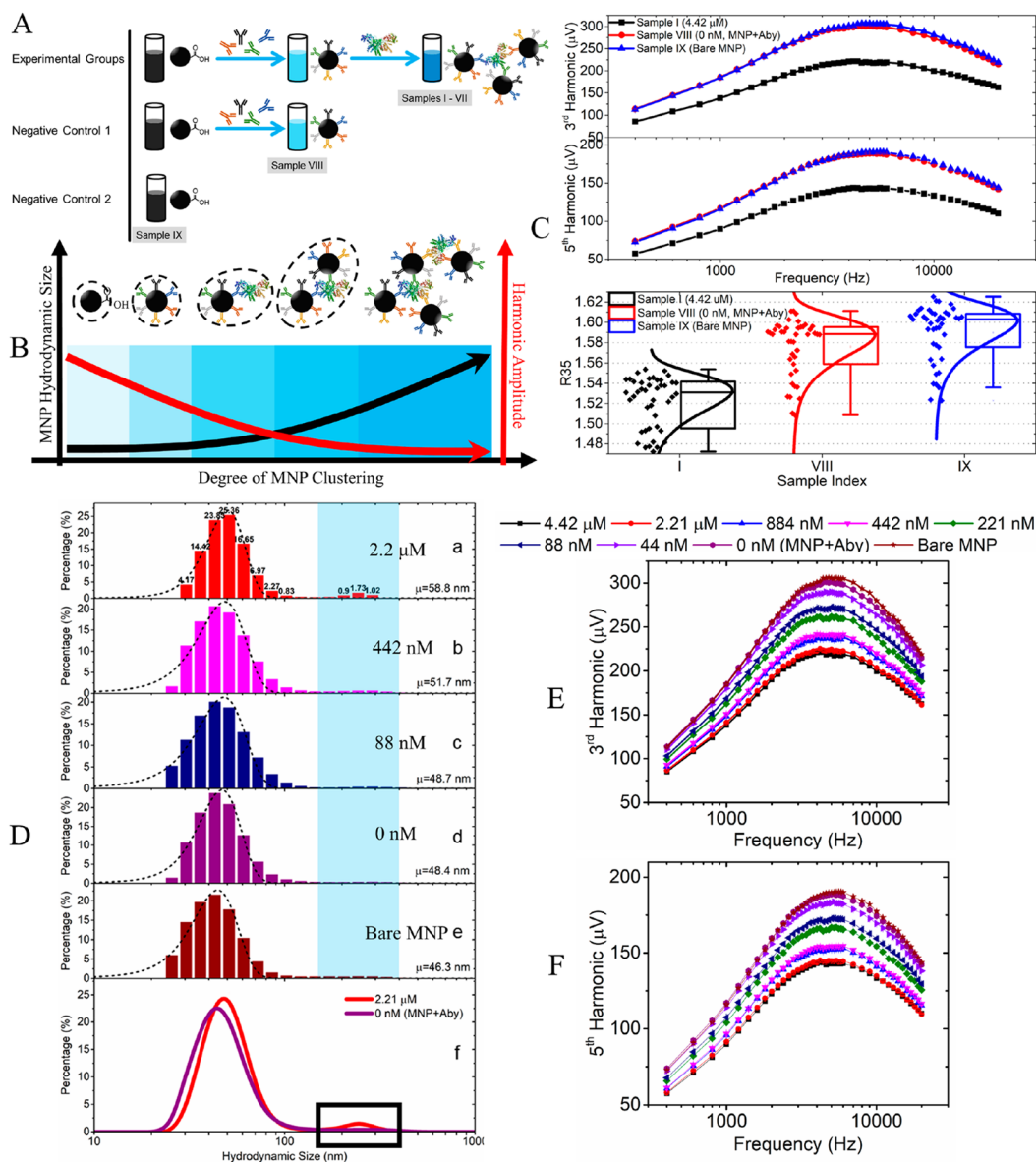
Figure 8. (A) Sample preparation flowcharts. (B) Harmonic amplitude drops and MNP hydrodynamic size increases as MNP forms clusters. (C) Example of the third and fifth harmonics along varying driving field frequencies collected by the MPS system. Boxplots show the harmonic ratios (R35) collected from samples I, VIII, and IX. (D) Statistical distribution of the hydrodynamic sizes of samples (a) II, (b) IV, (c) VI, (d) VIII, and (e) IX, as characterized by DLS. (f) Comparison of the measured DLS size distribution curves between samples II (2.21 μM) and VIII (0 nM, MNP + Aby). (E and F) MPS measurements of the third and fifth harmonics from samples I−IX at varying driving field frequencies from 400 Hz to 20 kHz. Reproduced from ref 87. Copyright 2020 American Chemical Society.

detection is the potential cross-reactivity of SARS-CoV-2 antibodies with antibodies generated against other coronaviruses.[26] Yet, in this work, cross-reactivity with another coronavirus such as MERS coronavirus (MERS-CoV) and SARS coronavirus (SARS-CoV) is not tested. This POC testing device allows for the identification of people with immunity against SARS-CoV-2.

3.3. Volume-Based MPS Platform. Zhang et al. first demonstrated the feasibility of using a volume-based MPS bioassay method for molecular sensing applications.[95] In their work, the MNPs are functionalized with two antithrombin DNA aptamers: the target analytes (i.e., thrombin) link MNPs together through DNA−DNA interactions, inhibiting the rotational freedom of MNPs and thus reducing the magnetic responses. They showed a LOD of 4 nM and 2 pmol for the

detection of thrombin. In addition, they also demonstrated the capability of detecting ssDNA from serum with a LOD of 400 pM. This pioneering work proves that volume-based MPS can be a promising platform for highly sensitive, versatile bioassay and potentially for future in vivo applications.

Wu et al. reported the volume-based MPS immunoassay platform utilizing the polyclonal-antibody-induced cross-linking of MNPs for one step, the wash-free detection of H1N1 nucleoprotein molecules.[87] In their work, the MNPs are anchored with polyclonal IgG antibodies specific to H1N1 nucleoprotein. Each H1N1 nucleoprotein molecule has many epitopes serving as binding sites for IgG polyclonal antibodies. Thus, each nucleoprotein can bind to more than one MNP, consequently forming MNP clusters. As shown in Figure 8A, seven experimental groups and two negative groups are
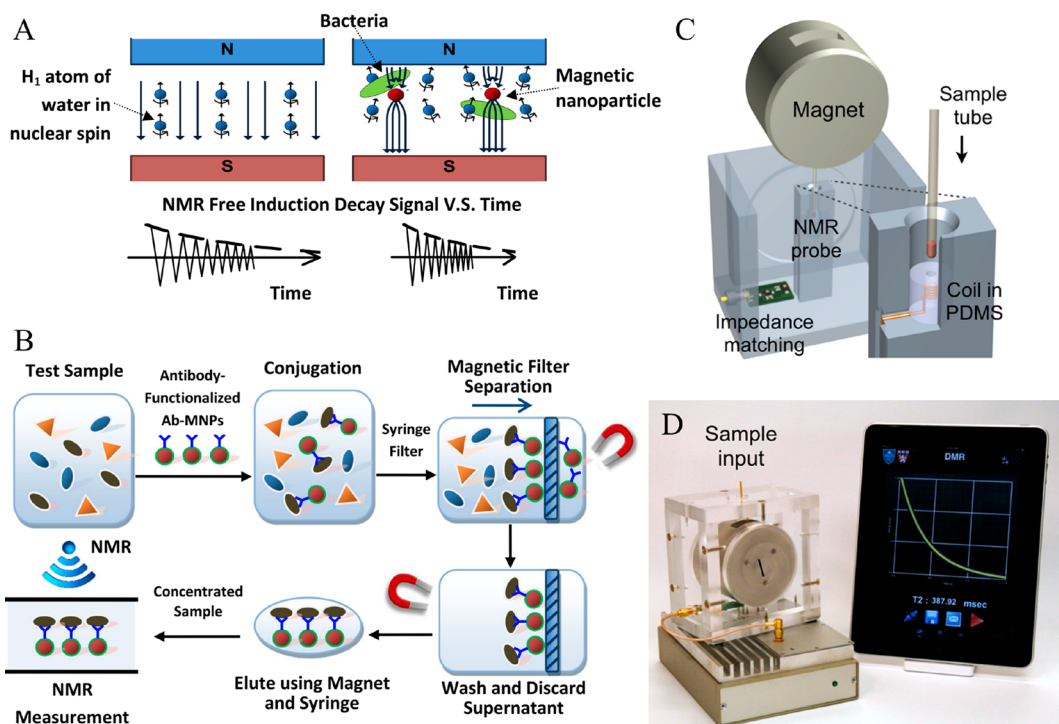
Figure 9. (A) MNP-induced spatial and temporal disturbances in the homogeneity and strength of the local magnetic field. (B) Schematic drawing of the working principle of the NMR-based biosensor for pathogen detection. (C) Schematic view of the magnet assembly and NMR probe design. (D) Photograph of a portable NMR device. The images in parts A and B adapted from ref 89 are licensed under CC BY-ND 2.0. Parts C and D were reproduced with permission from ref 134. Copyright 2011 The Royal Society of Chemistry.

prepared. For negative control 2 (sample index IX), magnetic responses of bare MNPs are recorded in the MPS platform. For negative control 1 (sample index VIII), the magnetic responses of polyclonal antibody–MNP complexes are recorded. For experimental groups I–VII, different concentrations of H1N1 nucleoprotein are mixed with polyclonal antibody–MNP complexes, and the concentrations from highest to lowest are 4.42 μM (I), 2.21 μM (II), 884 nM (III), 442 nM (IV), 221 nM (V), 88 nM (VI), and 44 nM (VII). Because of the varying abundancies of target analytes (i.e., H1N1 nucleoprotein), different degrees of MNP clustering are observed from samples I–VII. As shown in Figure 8B, with the increasing degree of MNP clustering, the averaged MNP hydrodynamic size increases and the harmonic amplitude decreases. Figure 8C shows the third- and fifth-harmonic amplitudes from samples IX, VIII, and I. With the anchoring of polyclonal antibodies onto MNPs, a small decrease in the harmonic amplitude is observed from sample VIII compared to sample IX, which proves the successful conjugation of antibodies on MNPs, and as a result, the hydrodynamic size slightly increases. The experimental group (sample I) shows a substantial decrease in the harmonic amplitudes due to H1N1-nucleoprotein-induced MNP clustering. As a side note, the harmonic ratios are also used as a MNP-quantity-independent factor for MPS-based immunoassay. Parts a–e of Figure 8D show the hydrodynamic size distributions of MNPs from samples II (2.21 μM), IV (442 nM), VI (88 nM), VIII (MNP–antibody complex), and IX (bare MNP) measured by dynamic light scattering (DLS). The hydrodynamic size increases after the anchoring of antibodies onto MNPs and then further increases in the presence of H1N1 nucleoprotein. Figure 8D,f gives a more intuitive comparison between samples II (2.21 μM) and VIII (MNP–

antibody complex). The H1N1 nucleoprotein causes a noticeable size peak shift from 46 to 59 nm. In addition, the bump between 200 and 300 nm indicates the presence of MNP clusters. In Figure 8E,F, the harmonic amplitudes recorded from samples I–IX show similar trends.

This one-step, wash-free, volume-based MPS detection scheme allows for immunoassay on minimally processed biological samples and handling by nontechnicians with minimum training requirements. Because the magnetic signals come for the whole volume of MNP suspension, removing the unbound MNPs from the sample could ensure higher detection sensitivity for this type of volume-based assay mode.

4. NMR PLATFORMS

4.1. NMR. The basic properties of NMR will be elaborated herein. Nuclei such as ^{1}H, ^{13}C, and ^{31}P with an odd number of protons and/or neutrons exhibit intrinsic magnetic moments and thus possess nonzero spin, where ^{1}H is the most studied nucleus because of its abundancy in biological samples. For example, the NMR signals from water and fat in the patient's tissues are monitored for MRI applications. When an external static magnetic field, H_0, is applied along the z direction, the nuclear spin behaves like a small magnetic bar and precesses about the field direction with a Larmor frequency. Upon removal of this external field, the nuclear spins are randomized, showing zero net magnetization on the macroscopic level. When a radio-frequency (RF) pulse is applied orthogonal to the static field H_0, these nuclei are flipped toward the x–y plane. A tipping angle of 90° (i.e., flipping the nuclear spins to the x–y plane) can maximize the resultant NMR signal in the transverse plane. When the RF pulse is removed, these nuclei relax back to equilibrium states. The RF coils monitor the transverse and longitudinal magnetizations of these nuclear
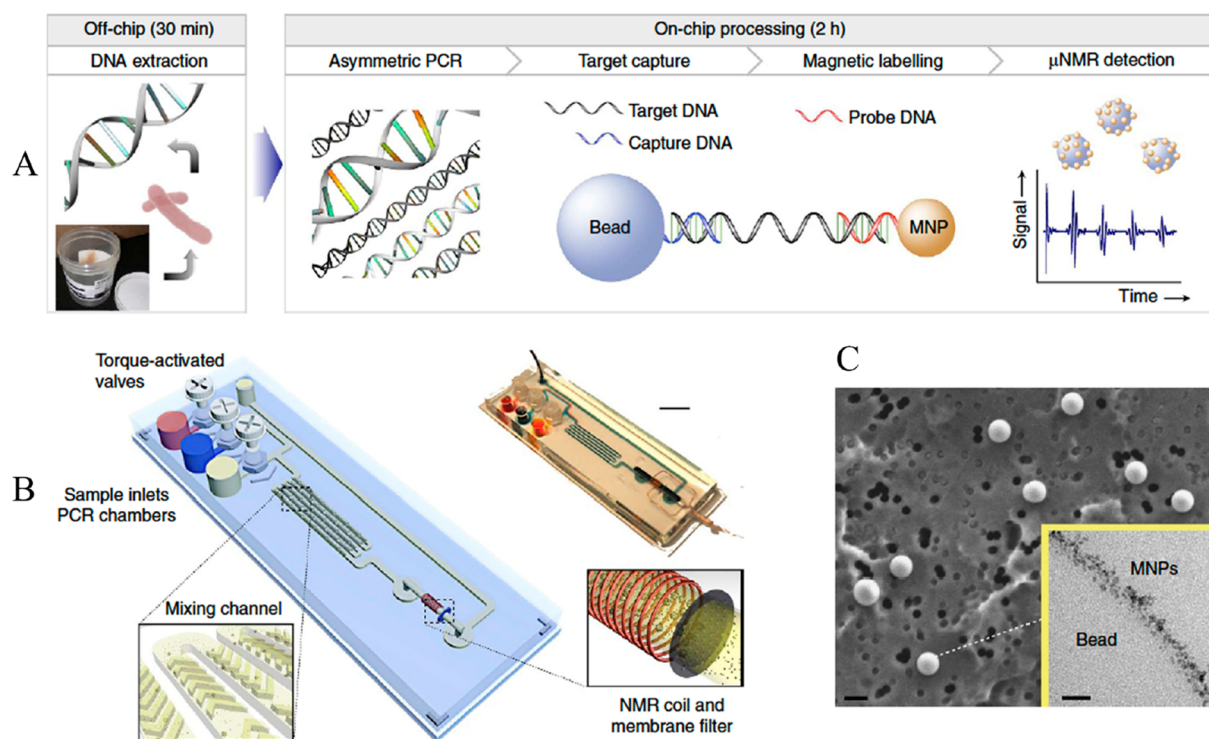
Figure 10. (A) Assay procedure. (B) Fluidic cartridge-integrating PCR chambers, a mixing channel, and a microcoil for NMR measurements. The entire cartridge is disposable. (C) SEM image of the bead captured by the membrane filter. Scale bar = 1 μm. The inset SEM image shows that the beads are efficiently labeled with MNPs. Scale bar = 30 nm. Reproduced with permission from ref 90. Copyright 2013 Springer Nature.

spins by means of measuring the magnetic flux. The longitudinal relaxation time T_1 is the time taken for the z-component of the nuclear spin (magnetization) to return to its thermal equilibrium value, and the transverse relaxation time T_2 is the measure of the decay of net magnetization in the $x-y$ plane (perpendicular to H_0). The reciprocals of T_1 and T_2 are known as the longitudinal and transverse relaxation rates R_1 and R_2, respectively.

For most bioassay applications, NMR detects the MNP-labeled targets by measuring the precessional signal of the ^{1}H proton from the whole sample volume. In this way, the NMR platform is categorized as one type of volume-based immunoassay method. Note that NMR-based immunoassay platform is also called magnetic relaxation switching. As shown in Figure 9A, because of the high surface-to-volume ratio of MNPs, the local magnetic field inhomogeneity caused by the MNP disturbs the precession frequency variations in millions of surrounding water protons, which accelerates the decay of the spin system's phase coherence. In addition, the NMR-based detection intrinsically benefits from signal amplification and is able to achieve high sensitivity. As the monodispersed MNPs aggregate upon binding to targets, the clusters can efficiently dephase the nuclear spins of the surrounding water protons, resulting in decreased T_2 relaxation time. The reverse is also true upon cluster disassembly. The magnetic relaxivity is defined as the intrinsic property of the MNP's ability to increase the longitudinal and transverse relaxation rates of its surrounding water protons. In order to optimize the MNPs for enhanced relaxivity of the water protons under a given field, the Solomon−Bloembergen−Morgan (SBM) theory was reported for the physical interpretation of nuclear spin relaxation in paramagnetic solutions.[117−119]

A highly homogeneous static field H_0 is the prerequisite for a high-sensitivity NMR platform. Such systems require highly homogeneous samples, coils, a container, and susceptibility matching, which are the major obstacles toward miniaturizing NMR.[120] In recent years, there have been many advances in miniaturizing the NMR platforms such as assembling electronics into integrated-circuit chips, implementing smaller or planar NMR coils and compact permanent magnets and mounting microfluidic channels.[120−130] These low-cost micro-NMR (μNMR) platforms have demonstrated the portability, robustness, versability, and even higher sensitivity than conventional systems. There are many books and reviews highlighting the recent advances of μNMR systems as well as the μNMR for real-life applications, and we list some of them for readers' information.[130−133]

Figure 9B shows the steps of NMR-based immunoassay with MNP−pathogen interaction, magnetic separation, and filtration. As mentioned in section 3.3, for volume-based biosensing platforms, the filtration step could effectively reduce the interference of unbound MNPs. The magnetic separation and filtration are not necessary but are favored for high-sensitivity immunoassays.

Issadore et al. reported a miniaturized NMR platform for POC diagnostics.[134] A photograph and the schematic of the portable NMR platform are shown in Figure 9C,D. The magnet, microcoils, and RF matching circuits are assembled into a thermally insulating shell. The circuits can provide NMR pulse sequences, collect NMR signals, and communicate with external terminals. Samples are loaded to polyimide tubes and inserted into the microcoil bore for NMR measurements. A modular coil is plugged into the system to accommodate sample volumes (i.e., from 1 to 100 mL). This portable NMR platform with automatic measurement setting tuning provides

Table 2. Advantages and Disadvantages of Different Magnetic Nanosensors

platform	advantages	disadvantages
GMR	high sensitivity	multiple washing steps usually required, thus needing well-trained technicians, but can be wash-free, which reduces the sensitivity
	availabilty of a portable device	time-consuming
	mass production capability	high cost per test; nanofabrication of GMR biosensors required
MTJ	high sensitivity	multiple washing steps usually required, thus needing well-trained technicians, but can be wash-free, which reduces the sensitivity
	mass production capability	high noise; large distance from the MNP to sensor surface
		hard-to-acquire linear response
		complicated fabrication process
		time-consuming
		high cost per test; nanofabrication of MTJ biosensors required
MPS, surface-based	high sensitivity	multiple washing steps usually required, thus needing well-trained technicians, but can be wash-free, which reduces the sensitivity
	low cost per test	time-consuming
	availabilty of a portable device	
MPS, volume-based	one-step wash-free detection allowed	medium sensitivity
	immunoassays that can be hand-held by nontechnicians	
	low cost per test	
	availabilty of a portable device	
NMR	availabilty of a portable device	multiple washing steps usually required, thus needing well-trained technicians, but can be wash-free, which reduces the sensitivity.
		time-consuming
		medium sensitivity

users with an easy-to-use interface and offers a sensitive on-site diagnosis. With these capabilities, it is expected that an NMR hand-held device can be an essential tool for personal care and accurate diagnostics for infectious diseases in rural areas and mitigates the healthcare burden.

4.2. NMR Platforms. Recent advances in micro- and nanofabrication have accelerated the development of portable NMR devices. Alocilja and Luo reported the detection of foodborne bacteria *E. coli O157:H7* from drinking water and milk samples using a portable NMR platform.[89] The NMR system is able to generate 0.47 T of magnetic field and a high-power pulsed RF transmitter with ultralow-noise-sensing circuitry. In their work, the bacteria are labeled with MNPs through antibody−pathogen interactions. A 20−30 min filtration step is carried out and followed by 1 min of NMR signal collection.

Liong et al. reported the detection of nucleic acids based on a magnetic barcoding strategy,[90] where the PCR-amplified mycobacterial genes are specifically captured on the microspheres and labeled by MNPs and then detected by the NMR technique. All of the components and steps are integrated into a fluidic cartridge for simplified on-chip assays. As shown in Figure 10A, the sputum samples are first processed to extract DNA from *M. tuberculosis* followed by PCR amplification. The amplicons are captured by polymeric beads that are coated with complementary capture DNA strands. Then MNPs modified with probed DNA strands bind to the other end of the amplicon. This capture DNA−target DNA−probe DNA scheme enhances the detection specificity and offers fast binding kinetics. After the removal of unbound MNPs, samples are subjected to NMR measurements. The MNPs captured due to target DNA cause faster relaxation of the ^{1}H NMR signal, and the decay rate is directly proportional of the MNP amount (and the amount of initial DNA), enabling the quantification of target DNA strands. The microfluid device for on-chip NMR measurements is shown in Figure 10B. MNPs

and buffers are preloaded in gated chambers, and after the target DNA strands are PCR-amplified, the amplicons are mixed with capture beads. The bead−DNA complexes are then mixed with MNPs and passed to the mixing channels. The MNP-labeled beads are filtered by an inline membrane, shown in Figure 10C, and concentrated into the NMR chamber for measurements.

In addition to the bioassay applications, saturation-transfer-difference (STD) NMR has emerged as a robust tool for characterizing protein binding and ligand screening.[135] It is used for identifying the underlying mechanisms of Hepatitis B virus X protein (HBx)-mediated carcinogenesis. Yue et al. used a NMR-based metabolomic approach to study the effects of HBx on cell metabolism.[136] Kusunoki et al. used NMR to characterize interactions between the HBx BH3-like motif and Bcl-$_{XL}$ and showed that this motif binds to the common BH3-binding hydrophobic groove of Bcl-$_{XL}$ with a binding affinity of 89 μM.[137] NMR is applied for assessing the ability of an artificially designed oligopeptide in binding to Ebola virus Viral Protein 24 (VP24).[138] The successful protein−protein binding could inhibit the interaction of Ebola virus VP24 with the human protein Karyopherin, thus reducing the Ebola virus virulence. Vasile et al. used NMR to study the interactions between the sialic acid and influenza hemagglutinin (HA) from human and avian strains.[139] Screening of the HA ligand−protein interactions could yield useful information for an efficient drug design.

Herein, we have reviewed different magnetic nanosensors and included the most representative literatures. The advantages and disadvantages of each platform are listed and compared in Table 2. It should be noted that the pros and cons listed in Table 2 are based technology but not on theoretical limiting values. There are several papers commenting on the limiting sensitivities of different magnetic nanosensors for readers' reference.[94,140−146]

Table 3. Magnetic Nanomaterials as Auxiliary Tools in Other Bioassay Platforms

platform	assay time	pathogen	LOD	evaluated matrix	function of magnetic nanomaterials	ref
MALDI-TOF MS	1 h	H5N2	$10^{4.5}$–$10^{5.5}$ TCID$_{50}$	virus lysate	magnetic separation	147
FMR	N.A.	V. cholerae	1 pM in a 1 μL sample	PBS	magnetic signal source	148
		Zika virus	100 aM in a 1 μL sample	PBS containing 20% fetal bovine serum		
RLS	12 h	HAV	6.2 pM	N.A.	magnetic separation and magnetic signal source	150
	20 min	JEV	1.3 pM	serum	magnetic separation and magnetic signal source	151
SERS	25 min	H3N2	10^2 TCID$_{50}$/mL in a 100 μL sample	PBS	SERS-active magnetic supporting substrates	152
RT-PCR	2 h	HBV	10 copies in a 1 μL sample	serum	magnetic separation	154
		HCV	10 copies in a 1 μL sample			
		HIV	100 copies in a 1 μL sample			
fluorometry	2 h	EIV	1.3 ng/mL EIV antigen	PBS	magnetic separation	153
		EIAV	1.2 ng/mL EIAV antigen			
	30 min	E. coli	N.A.	PBS	fluorescence quenching and magnetic separation	155
		S. aureus				
	N.A.	alternaria species	0.25 pg/mL for AME	PBS	magnetic separation	157
	1 h	HTLV-II	0.22 fM for DNA detection	serum	magnetic separation	158

To evaluate a bioassay platform, the assay sensitivity (positive percent agreement) and specificity (negative percent agreement) are usually of interest. Sensitivity refers to the bioassay platform's ability to correctly detect the sick people who do have the illness. This parameter is determined by both the concentration level of target analytes from the sample and the volume of the sample available for testing. In addition, a bioassay platform should be sufficiently sensitive so that the concentration/quantity level of target analytes falls withing the dynamic range of the assay. The sensitivity of a platform can be increased when coupled with amplification techniques (such as RT-PCR) when nucleic acids are detected. Thus, the assay sensitivity of a platform depends on the intrinsic property of the sensor: the dynamic range. External factors such as the sample volume available for testing, whether it is coupled with amplification techniques, can also affect the platform sensitivity. Thus, in Table 2, the sensitivity of each bioassay platform is only evaluated by its intrinsic sensitivity without considering external factors.

On the other hand, the specificity is that the assay will measure only the target analytes and not the substrate or any other analytes. Steps can be taken to improve the assay specificity. Taking the antibody−antigen-based immunoassay as an example, it is desired to obtain antibodies that are of high-binding specificity and affinity to target analytes. Such antibodies must be characterized rigorously under actual assay conditions to ensure that they have the desired specificity. In addition, the high bioassay specificity is often difficult to reach when testing from a complex sample matrix. For example, the one-step wash-free assay method might suffer from lower assay specificity. Thus, assay specificity of a platform depends on external factors such as antibodies and the assay format. This is the reason why the assay specificity of each platform is not listed or compared in Table 2.

5. OTHER MAGNETIC BIOASSAY METHODS

In most magnetic nanosensors, MNPs are used as labels (e.g., MR sensors and MPS platforms) or contrast enhancers (e.g., NMR

platforms) because of their unique magnetic properties, large surface-to-volume ratio, good stability and biocompatibility, and facile surface functionalization with a great variety of reagents. In addition to the above technologies, other platforms that utilize MNPs as auxiliary tools for virus and pathogen detection have also been extensively reported. In this section, we reviewed some representative works that use magnetic nanomaterials as auxiliary tools for high-sensitivity virus and pathogen detection, as summarized in Table 3.

Chou et al. use surface-functionalized MNPs as probes for efficient magnetic separation to achieve rapid and sensitive virus screening.[147] In their work, MNPs are functionalized with H5N2 viral antibodies targeting the HA protein. Combined with magnetic separation, these MNPs show effective isolation of H5N2 from lysate for direct matrix-assisted laser desorption/ionization time-of-flight mass spectrometry (MALDI-TOF MS) readout without any elution steps. A LOD in the range of $10^{4.5}$–$10^{5.5}$ TCID$_{50}$ is achieved within a diagnosis time of 1 h. The functionalized MNP probes can unambiguously differentiate the H5N2 viruses from other subtypes such as H5N1 viruses with a high specificity and thus can be utilized for the rapid screening of different virus subtypes.

Tian et al. reported ferromagnetic resonance (FMR)-based volumetric and homogeneous biosensors for DNA detection.[148] This method quantifies the target DNA by measuring the FMR field shift of the suspension. The detection strategy for target DNA is based on an isothermal amplification followed by hybridization with detection-antibody-modified MNPs. In the presence of target DNA strands, antibody−MNP complexes form aggregates, which lowers the net anisotropy as well as increases of the resonance field. For rolling circle amplification (RCA)-based FMR assays, a LOD of 1 pM and a linear detection range of 7.8−250 pM are obtained for detecting synthetic Vibrio cholerae target DNA from buffer solutions. For loop-mediated-isothermal-amplification-based FMR assays, a LOD of 100 aM is obtained for the detection of a synthetic Zika virus target oligonucleotide from 20% serum samples.

Barrios-Gumiel et al. reported carbosilane-dendron-decorated MNPs with peripheral carboxyl and carboxylate groups for the capture and concentration of R5-HIV-1$_{NLAD8}$ and X4-HIV-1$_{NL4.3}$ strains.[149] The carboxyl and carboxylate MNPs assist in achieving rapid and easy diagnostics and reduce/eliminate the risk of HIV-1 transmission.

Zhang et al. synthesized a virus magnetic−molecularly imprinted polymer (MIP) complex under an applied magnetic field.[150] The existence of Fe$_3$O$_4$ MNPs can accelerate the preparation process of

the complex. Because the viruses were captured specifically to the surface of the magnetic−MIP, the size and shape of the particles changed, leading to a change in the magnetic resonance light scattering (RLS) signal. The linear concentration range for hepatitis A virus was 0.02−1.4 nM, with a LOD of 6.2 pM. A similar setup was also employed to detect the Japanese encephalitis virus (JEV) with a LOD of 1.3 pM in human serum.[151]

Furthermore, MNPs have been frequently coupled with several other nonmagnetic materials such as Au, silica, fluorescent pores, and quantum dots (QDs) in different bioassay platforms.

Sun et al. reported a magnetic immunoassay method based on surface-enhanced Raman scattering (SERS) spectroscopy to detect influenza virus H3N2 (A/Shanghai/4084T/2012) through a sandwich-structure complex consisting of SERS tags, the target influenza virus, and Fe_3O_4/Au MNPs as supporting and capturing substrates.[152] Using a portable Raman spectrometer, a LOD of 10^2 $TCID_{50}$/mL and linear detection range of 10^2−5×10^3 $TCID_{50}$/mL are achieved.

Wang et al. employed two kinds of labels for the virus antibody and antigen separately.[153] The virus antigens were functionalized with fluorescent-encoded MNPs, while the antibodies were conjugated to green-emitting CdTe QDs. Through the application of different kinds of fluorescent nanocomposites to the antigens, multiplexed detection of equine influenza virus (EIV) and equine infectious anemia virus (EIAV) was achieved with sensitivities of 1.3 and 1.2 ng/mL for EIV and EIAV antigens, respectively.

Ali et al. employed MNPs in a RT-PCR platform for multiplexed detection of HBV, hepatitis C virus (HCV), and human immunodeficiency virus (HIV).[154] Silica-coated MNPs were used during nucleic acid extraction. After the RT-PCR process, the viruses were then captured by MNPs coated with amino-modified probes and carboxyl. Multiplexed detection was realized with the ability to detect less than 100 copies of viruses per microliter of serum.

Zong et al. conjugated three different fluorescent proteins (FPs) to a MNP. Upon interaction with target bacteria, characteristic levels of these FPs are displaced depending on the binding strength among quaternized MNPs, FPs, and bacteria.[155] The excitation/emission wavelengths of these FPs are 380/450, 480/510, and 555/585 nm for blue, green, and red fluorescent proteins, respectively. The fluorescence response patterns are analyzed by principle component analysis and linear discriminant analysis. This technology can rapidly detect and distinguish different types of bacteria with an 89.7% first discriminant within 30 min.

Kim et al. reported the detection of cathepsin L (associated with some cancer cells) by controlling the aggregations of polymer dots (CPdots) and MNPs.[156] In the presence of cathepsin L, the fluorescence and MRI relaxivity are changed because of the aggregations of CPdots and MNPs. This detection method can also be applied in virus and pathogen detection.

Man et al. reported fluorometric immunoassay by introducing H_2O_2-mediated fluorescence quenching of mercaptopropionic acid-capped CdTe QDs (MPA-CdTe QDs) into MNP-based immunoassay for the detection of alternariol monomethyl ether (AME).[157] AME is a mycotoxin produced by the Alternaria species. Herein, free AME from the sample competes with catalase (CAT)-labeled AME to bind to monoclonal antibodies (mAbs) on MNPs. Quenching of the fluorescence of MPA-CdTe QDs can be used to quantify AME from the sample. However, because of the large scale of detection instruments and the complexity of sample preparation, all of the reported AME detection methods are only used in laboratory setups.

Zheng et al. developed a fluorescent biosensor for the detection of human T-lymphotropic virus type II (HTLV-II) DNA based on MNPs and atom-transfer radical polymerization (ATRP) signal amplification.[158] The good performance of this biosensor is mainly due to the ATRP signal amplification, magnetic separation of MNPs, and high specificity of the DNA strands. In this study, they utilized the fluorescent substance 9-anthracenylmethyl methacrylate polymer (pAMMA) as the signal reporting unit and hairpin DNA as the capture probe for the detection of HTLV-II DNA. To be specific, MNPs are modified with hairpin DNA probes (pDNA), in the presence of target DNA (tDNA), pDNA hybridizes with tDNA, and therefore the hairpin structure opens and the azide group is pushed away from the MNP. Then initiators are introduced into pDNA by a Cu(I)-catalyzed alkyne−azide cycloaddition reaction in order to initiate the ATRP reaction. Afterward, pAMMA is anchored on the MNPs to generate long polymeric chains, thus amplifying the fluorescence signal and improving the detection sensitivity.

MR sensors discussed in section 2 have been the most popular magnetic bioassay technique. However, these nanodevices suffer from high background noise, which hinders the sensitivity of these biosensors at room temperature. Tian et al. reported the volumetric detection of DNA using FMR shifts.[148] Aggregation of MNPs was caused by binding of the V. cholerae target DNA sequence, which gave rise to significant FMR shifts compared to nonaggregated MNPs. However, this technique involves the insertion of MNP samples inside an electromagnetic cavity, which is not nanoscale-frequency detection. The first feasibility of nanoscale-frequency-based biodetection was made by a group from University of Western Australia. However, their work, including both simulation and experimental demonstrations, was restricted to the detection of MNPs using magnonic crystals and nanodots.[159−161] The physics behind the operation of such devices is that, at nanoscale, the FMR frequency of the device interacts directly with the dipolar fields from MNPs, which, as a result, triggers a shift in the peak frequency. The main advantage of the frequency-based approach over the MR-based technique is that the frequency of the operation of these devices is high (on the order of terahertz), and hence there is a significant reduction of the $1/f$ noise. On this basis, Saha et al. for the first time demonstrated the feasibility of a frequency-based biosensor through a simulation study.[162] This work showed the feasibility of using a spin-current nanooscillator device as a frequency-based biosensor. It pointed out how the frequency-based biosensor is position-sensitive, in addition to demonstrating room temperature single molecular sensitivity. Furthermore, Bai et al., very recently, demonstrated the terahertz sensing of HeLa cells Pseudomonas, which is based on monolithic integrated metamaterials as spintronic terahertz emitters.[163] A spintronic emitter made of W/CoFeB/Pt offers the possibility of an extremely low-cost, near-field terahertz, label-free biosensor option with high sensitivity and high spatial resolution. The fact that this terahertz biosensor is label-free significantly reduces the cost for purchasing the biomarkers, magnetic labels, or MNPs.

6. DISCUSSIONS

6.1. LOD. This review paper focuses on magnetic nanosensors for pathogen and virus detection, and different detection tools are reported and categorized in Table 1. It should be noted that, in the context of LOD, it is much easier to detect viruses/bacteria than small molecules (i.e., antigens, antibodies). Small molecules such as antigens host fewer binding sites for magnetic labels (i.e., MNPs), while a single virus/bacterium might host hundreds or thousands of binding sites depending on what is targeted. Thus, the sensitivity will be amplified dramatically when small-molecule detection methods are used on viruses/bacteria.

6.2. Detection Platforms Categorized by Target Biomarkers. Detection platforms can also be categorized by the target biomarkers such as nucleic acid and protein testing (protein antigens and antibodies). Other nonmagnetic diagnostic tools such as computed tomography scans and nucleic acid analysis are prevalently used for diagnosing and screening COVID-19.[164−168] In the end, however, a very basic question still lingers in our mind: Where are these nansensors when the world is fighting a global health pandemic? Why are they not being put to commercialization? This can be answered from several points of view. From a technical view, an ideal biosensor should meet most or all of the following requirements: high sensitivity, high selectivity, fast, multi-

plexing capabilities, multiple sensing modes, disposability, long shelf-life, and user friendliness. Pros and cons for the magnetic biosensors given in Table 2 clearly indicate that all technologies lack something or other from the technical point of view. Furthermore, advancements in the bioassay platform require investments from industry for the particular technology to be mass-manufacturable, autonomous, and cost-effective. So far, magnetic biosensors have not been commercialized to a very large extent. That is why portable magnetic nanosensors have not been a big shot in the midst of this global pandemic.

6.3. Biological Sample Preparation Method for Different Target Biomarkers. Herein, we briefly introduce the biological sample preparation methods for detecting different biomarkers. The preparation methods for detecting nucleic acid, antigens, and antibodies of SARS-CoV-2 are described as follows:

Extraction of Nucleic Acid and Antigens of SARS-CoV-2 from Nasal- and Nasopharyngeal-Swab Samples. In general, nasal- and nasopharyngeal-swab samples are placed in universal or viral transport media after collection. Before testing, samples are subjected to mixing by vortexing. For nucleic acid detection, a specific volume of the specimen eluted from the swab is used to extract RNA by commercial RNA extraction reagents. For antigen detection, the specimen eluted from the swab is directly used without further extraction.

Extraction of Antibodies of SARS-CoV-2 from Blood Samples. For antibody detection, whole blood, serum, or plasma are used. In general, whole blood is processed into serum or plasma for storage if not analyzed on the same day. Serum is generated by leaving whole blood at room temperature after collection for about 30 min to clot. Blood is then centrifuged to separate clear serum from the clot. For plasma, whole blood is collected in a sterile tube containing an anticoagulant. Plasma is then separated from the remaining blood cells by centrifugation.

6.4. Magnetic Nanosensor-Based POC Devices on the Market. To the best of our knowledge, as of July 2020, there are three companies applying GMR platforms for real-life disease diagnosis including Zepto Life Technology, LLC. (St. Paul, MN), Dongguan Bosh Biotechnologies, Ltd. (Guangdong Province, China), and Flux BioscFlux Biosciences, Inc. (San Francisco, CA). Recently, T2 Biosystems, Inc. (Lexington, MA), a company developing NMR-based disease diagnosis platforms, has released the T2SARS-CoV-2 Panel in response to the COVID-19 pandemic. The Panel now is commercially available and has been validated in accordance with Emergency Use Authorization requirements from the Food and Drug Administration (FDA). It is currently being distributed in accordance with FDA guidance.

7. CONCLUSIONS AND PERSPECTIVES

In summary, in the midst of the COVID-19 pandemic, the demand for highly sensitivity, lower-cost, rapid, easy-to-use, and reliable disease testing tools is increasing. Current diagnostic tests for SARS-CoV-2, the virus responsible for COVID-19, are based on real-time RT-PCR assay. Although it is sensitive, PCR requires trained technicians to perform the tests and has long turnaround times. While PCR strategies are limited to the detection of nucleic acids, magnetic nanosensors are more versatile and can be applied for antigen, antibody, and nucleic acid detection. Magnetic nanosensor platforms are often overlooked compared to the traditional optical, electro-

chemical, and mechanical sensors. Furthermore, POC devices based on magnetic nanosensors are delayed when it comes to commercialization despite their promising high sensitivity and simple operation. A common disadvantage of most magnetic nanosensor platforms is the fact that they rely on the use of magnetic labels for detection and/or separation. Although magnetic labels are advantageous over the optical and electrochemical techniques that use fluorescent dyes, unstable enzymes, and radioisotopes in terms of biocompatibility and stability in different biological environments, the requirement for a label in the detection process could hinder many in vivo applications as well as introduce additional complexity.[169,170] For bioassay applications, the sizes of the magnetic labels are required to be comparable to the analyte molecules. With nanoscale size, these magnetic labels suffer from small magnetic moment, nonuniform size distribution, which may cause signal variations especially for the detection of ultralow amounts of target analytes, severe surface defects caused by the large surface-to-volume ratio, and undesirable thermal heating. Optimization of the magnetic labels, improvement of the magnetic sensitivity, and the development of label-free magnetic biosensors are needed in the future to make magnetic POC platforms more competitive in the market. In general, magnetic nanosensor platforms benefit from easier sample preparation compared to optical techniques, use safer magnetic labels compared to electrochemical techniques, and are capable of homogeneous detection compared to mechanical techniques. In view of these advantages, we can expect them to supplant or supplement the current diagnosis techniques that rely on nonmagnetic strategies. Furthermore, researchers in the field of magnetic nanosensors are making significant progress toward expanded POC devices.[169,171]

As of July 2020, there is no effective vaccine to prevent the spread of COVID-19. As researchers worldwide search for effective cures for COVID-19, actions are also being taken to search for better and faster diagnosis tools for the timely diagnosis, management, and control of COVID-19. We reviewed the magnetic nanosensor literatures prior to COVID-19 and highlighted some promising tools for the detection of pathogens as well as viruses with high specificity and sensitivity. All of the detection platforms reviewed in this paper can be extended to the detection of other microorganisms and/or viruses with a change in the reagents on MNPs. It is expected that magnetic nanosensors will reform today's expensive and labor-intensive diagnostics and make cost-effective, user-friendly detection protocols possible, with superior/comparable sensitivity. This paradigm shift could contribute to better surveillance and control of SARS-CoV-2 infection in populations.

■ AUTHOR INFORMATION

Corresponding Authors

Kai Wu — *Department of Electrical and Computer Engineering, University of Minnesota, Minneapolis, Minnesota 55455, United States;* ● orcid.org/0000-0002-9444-6112; Email: wuxx0803@umn.edu

Maxim C.-J. Cheeran — *Department of Veterinary Population Medicine, University of Minnesota, St. Paul, Minnesota 55108, United States;* ● orcid.org/0000-0002-5331-4746; Email: cheeran@umn.edu

Jian-Ping Wang — *Department of Electrical and Computer Engineering, University of Minnesota, Minneapolis, Minnesota*

55455, United States; ● orcid.org/0000-0003-2815-6624;
Email: jpwang@umn.edu

Authors

Renata Saha − *Department of Electrical and Computer
Engineering, University of Minnesota, Minneapolis, Minnesota
55455, United States;* ● orcid.org/0000-0002-0389-0083

Diqing Su − *Department of Chemical Engineering and Material
Science, University of Minnesota, Minneapolis, Minnesota
55455, United States;* ● orcid.org/0000-0002-5790-8744

Venkatramana D. Krishna − *Department of Veterinary
Population Medicine, University of Minnesota, St. Paul,
Minnesota 55108, United States;* ● orcid.org/0000-0002-
1980-5525

Jinming Liu − *Department of Electrical and Computer
Engineering, University of Minnesota, Minneapolis, Minnesota
55455, United States;* ● orcid.org/0000-0002-4313-5816

Complete contact information is available at:
https://pubs.acs.org/10.1021/acsanm.0c02048

Notes
The authors declare no competing financial interest.

■ REFERENCES

(1) Lu, H.; Stratton, C. W.; Tang, Y.-W. Outbreak of Pneumonia of Unknown Etiology in Wuhan, China: The Mystery and the Miracle. *J. Med. Virol.* **2020**, *92* (4), 401−402.

(2) Zhu, N.; Zhang, D.; Wang, W.; Li, X.; Yang, B.; Song, J.; Zhao, X.; Huang, B.; Shi, W.; Lu, R. A Novel Coronavirus from Patients with Pneumonia in China, 2019. *N. Engl. J. Med.* **2020**, *382*, 727.

(3) Wu, F.; Zhao, S.; Yu, B.; Chen, Y.-M.; Wang, W.; Song, Z.-G.; Hu, Y.; Tao, Z.-W.; Tian, J.-H.; Pei, Y.-Y.; et al. A New Coronavirus Associated with Human Respiratory Disease in China. *Nature* **2020**, *579* (7798), 265−269.

(4) of the International, C. S. G. The Species Severe Acute Respiratory Syndrome-Related Coronavirus: Classifying 2019-NCoV and Naming It SARS-CoV-2. *Nat. Microbiol.* **2020**, *5*, (4), 536.

(5) Zhou, P.; Yang, X.-L.; Wang, X.-G.; Hu, B.; Zhang, L.; Zhang, W.; Si, H.-R.; Zhu, Y.; Li, B.; Huang, C.-L.; et al. A Pneumonia Outbreak Associated with a New Coronavirus of Probable Bat Origin. *Nature* **2020**, *579* (7798), 270−273.

(6) Chan, J. F.-W.; Kok, K.-H.; Zhu, Z.; Chu, H.; To, K. K.-W.; Yuan, S.; Yuen, K.-Y. Genomic Characterization of the 2019 Novel Human-Pathogenic Coronavirus Isolated from a Patient with Atypical Pneumonia after Visiting Wuhan. *Emerging Microbes Infect.* **2020**, *9* (1), 221−236.

(7) Khailany, R. A.; Safdar, M.; Ozaslan, M. Genomic Characterization of a Novel SARS-CoV-2. *Gene Rep.* **2020**, *19*, 100682.

(8) Sawicki, S. G.; Sawicki, D. L.; Siddell, S. G. A Contemporary View of Coronavirus Transcription. *J. Virol.* **2007**, *81* (1), 20−29.

(9) Chen, N.; Zhou, M.; Dong, X.; Qu, J.; Gong, F.; Han, Y.; Qiu, Y.; Wang, J.; Liu, Y.; Wei, Y.; et al. Epidemiological and Clinical Characteristics of 99 Cases of 2019 Novel Coronavirus Pneumonia in Wuhan, China: A Descriptive Study. *Lancet* **2020**, *395* (10223), 507−513.

(10) Huang, C.; Wang, Y.; Li, X.; Ren, L.; Zhao, J.; Hu, Y.; Zhang, L.; Fan, G.; Xu, J.; Gu, X.; et al. Clinical Features of Patients Infected with 2019 Novel Coronavirus in Wuhan, China. *Lancet* **2020**, *395* (10223), 497−506.

(11) Wang, D.; Hu, B.; Hu, C.; Zhu, F.; Liu, X.; Zhang, J.; Wang, B.; Xiang, H.; Cheng, Z.; Xiong, Y.; et al. Clinical Characteristics of 138 Hospitalized Patients with 2019 Novel Coronavirus−Infected Pneumonia in Wuhan, China. *Jama* **2020**, *323* (11), 1061−1069.

(12) Corman, V. M.; Landt, O.; Kaiser, M.; Molenkamp, R.; Meijer, A.; Chu, D. K.; Bleicker, T.; Brünink, S.; Schneider, J.; Schmidt, M. L.; et al. Detection of 2019 Novel Coronavirus (2019-NCoV) by Real-Time RT-PCR. *Eurosurveillance* **2020**, *25* (3), 2000045.

(13) Chu, D. K.; Pan, Y.; Cheng, S. M.; Hui, K. P.; Krishnan, P.; Liu, Y.; Ng, D. Y.; Wan, C. K.; Yang, P.; Wang, Q.; Peiris, M.; Poon, L. L. M. Molecular Diagnosis of a Novel Coronavirus (2019-NCoV) Causing an Outbreak of Pneumonia. *Clin. Chem.* **2020**, *66* (4), 549−555.

(14) Kucirka, L. M.; Lauer, S. A.; Laeyendecker, O.; Boon, D.; Lessler, J. Variation in False-Negative Rate of Reverse Transcriptase Polymerase Chain Reaction-Based SARS-CoV-2 Tests by Time since Exposure. *Ann. Intern. Med.* **2020**, *173*, 262.

(15) Qin, C.; Liu, F.; Yen, T.-C.; Lan, X. 18 F-FDG PET/CT Findings of COVID-19: A Series of Four Highly Suspected Cases. *Eur. J. Nucl. Med. Mol. Imaging* **2020**, *47*, 1281−1286.

(16) Li, D.; Wang, D.; Dong, J.; Wang, N.; Huang, H.; Xu, H.; Xia, C. False-Negative Results of Real-Time Reverse-Transcriptase Polymerase Chain Reaction for Severe Acute Respiratory Syndrome Coronavirus 2: Role of Deep-Learning-Based CT Diagnosis and Insights from Two Cases. *Korean J. Radiol.* **2020**, *21* (4), 505−508.

(17) Zhao, J.; Yuan, Q.; Wang, H.; Liu, W.; Liao, X.; Su, Y.; Wang, X.; Yuan, J.; Li, T.; Li, J. et al. Antibody Responses to SARS-CoV-2 in Patients of Novel Coronavirus Disease 2019. *Clin. Infect. Dis.* **2020**. DOI: 10.1093/cid/ciaa344

(18) Arevalo-Rodriguez, I.; Buitrago-Garcia, D.; Simancas-Racines, D.; Zambrano-Achig, P.; del Campo, R.; Ciapponi, A.; Sued, O.; Martinez-Garcia, L.; Rutjes, A.; Low, N. False-Negative Results of Initial RT-PCR Assays for COVID-19: A Systematic Review. *medRxiv* **2020**.

(19) Zhen, W.; Smith, E.; Manji, R.; Schron, D.; Berry, G. J. Clinical Evaluation of Three Sample-to-Answer Platforms for the Detection of SARS-CoV-2. *J. Clin. Microbiol.* **2020**. *58* DOI: 10.1128/JCM.00783-20

(20) Basu, A.; Zinger, T.; Inglima, K.; Woo, K.; Atie, O.; Yurasits, L.; See, B.; Aguero-Rosenfeld, M. E. Performance of Abbott ID NOW COVID-19 Rapid Nucleic Acid Amplification Test in Nasopharyngeal Swabs Transported in Viral Media and Dry Nasal Swabs, in a New York City Academic Institution. *J. Clin. Microbiol.* **2020**. DOI: 10.1128/JCM.01136-20

(21) Mitchell, S. L.; George, K. S. Evaluation of the COVID19 ID NOW EUA Assay. *J. Clin. Virol.* **2020**, *128*, 104429.

(22) Amanat, F.; Stadlbauer, D.; Strohmeier, S.; Nguyen, T. H.; Chromikova, V.; McMahon, M.; Jiang, K.; Arunkumar, G. A.; Jurczyszak, D.; Polanco, J.; et al. A Serological Assay to Detect SARS-CoV-2 Seroconversion in Humans. *Nat. Med.* **2020**, *26*, 1033−1036.

(23) Beavis, K. G.; Matushek, S. M.; Abeleda, A. P. F.; Bethel, C.; Hunt, C.; Gillen, S.; Moran, A.; Tesic, V. Evaluation of the EUROIMMUN Anti-SARS-CoV-2 ELISA Assay for Detection of IgA and IgG Antibodies. *J. Clin. Virol.* **2020**, *129*, 104468.

(24) Liu, R.; Liu, X.; Yuan, L.; Han, H.; Shereen, M. A.; Zhen, J.; Niu, Z.; Li, D.; Liu, F.; Wu, K.; luo, Z.; Zhu, C. Analysis of Adjunctive Serological Detection to Nucleic Acid Test for Severe Acute Respiratory Syndrome Coronavirus 2 (SARS-CoV-2) Infection Diagnosis. *Int. Immunopharmacol.* **2020**, *86*, 106746.

(25) Zhang, W.; Du, R.-H.; Li, B.; Zheng, X.-S.; Yang, X.-L.; Hu, B.; Wang, Y.-Y.; Xiao, G.-F.; Yan, B.; Shi, Z.-L.; Zhou, P. Molecular and Serological Investigation of 2019-NCoV Infected Patients: Implication of Multiple Shedding Routes. *Emerging Microbes Infect.* **2020**, *9* (1), 386−389.

(26) Lv, H.; Wu, N. C.; Tsang, O. T.-Y.; Yuan, M.; Perera, R. A.; Leung, W. S.; So, R. T.; Chan, J. M. C.; Yip, G. K.; Chik, T. S. H.; et al. Cross-Reactive Antibody Response between SARS-CoV-2 and SARS-CoV Infections. *Cell Rep.* **2020**, *31*, 107725.

(27) Liu, R.; Fu, A.; Deng, Z.; Li, Y.; Liu, T. Promising Methods for Detection of Novel Coronavirus SARS-CoV-2. *View* **2020**, *1* (1), No. e4.

(28) Xie, C.; Jiang, L.; Huang, G.; Pu, H.; Gong, B.; Lin, H.; Ma, S.; Chen, X.; Long, B.; Si, G. Comparison of Different Samples for 2019 Novel Coronavirus Detection by Nucleic Acid Amplification Tests. *Int. J. Infect. Dis.* **2020**, *93*, 264.

(29) Pang, J.; Wang, M. X.; Ang, I. Y. H.; Tan, S. H. X.; Lewis, R. F.; Chen, J. I.-P.; Gutierrez, R. A.; Gwee, S. X. W.; Chua, P. E. Y.; Yang, Q.; et al. Potential Rapid Diagnostics, Vaccine and Therapeutics for 2019 Novel Coronavirus (2019-NCoV): A Systematic Review. *J. Clin. Med.* **2020**, *9* (3), 623.

(30) Wang, M.; Fu, A.; Hu, B.; Tong, Y.; Liu, R.; Liu, Z.; Gu, J.; Xiang, B.; Liu, J.; Jiang, W.; et al. Nanopore Targeted Sequencing for the Accurate and Comprehensive Detection of SARS-CoV-2 and Other Respiratory Viruses. *Small* **2020**, *16* (32), 2002169.

(31) Shan, B.; Broza, Y. Y.; Li, W.; Wang, Y.; Wu, S.; Liu, Z.; Wang, J.; Gui, S.; Wang, L.; Zhang, Z. Multiplexed Nanomaterial-Based Sensor Array for Detection of COVID-19 in Exhaled Breath. *ACS Nano* **2020**, *14*, 12125.

(32) Su, D.; Wu, K.; Krishna, V.; Klein, T.; Liu, J.; Feng, Y.; Perez, A. M.; Cheeran, M. C.; Wang, J.-P. Detection of Influenza a Virus in Swine Nasal Swab Samples With a Wash-Free Magnetic Bioassay and a Handheld Giant Magnetoresistance Sensing System. *Front. Microbiol.* **2019**, *10*, 1077.

(33) Rettcher, S.; Jungk, F.; Kühn, C.; Krause, H.-J.; Nölke, G.; Commandeur, U.; Fischer, R.; Schillberg, S.; Schröper, F. Simple and Portable Magnetic Immunoassay for Rapid Detection and Sensitive Quantification of Plant Viruses. *Appl. Environ. Microbiol.* **2015**, *81* (9), 3039−3048.

(34) Aytur, T.; Foley, J.; Anwar, M.; Boser, B.; Harris, E.; Beatty, P. R. A Novel Magnetic Bead Bioassay Platform Using a Microchip-Based Sensor for Infectious Disease Diagnosis. *J. Immunol. Methods* **2006**, *314* (1), 21−29.

(35) Hash, S.; Martinez-Viedma, M. P.; Fung, F.; Han, J. E.; Yang, P.; Wong, C.; Doraisamy, L.; Menon, S.; Lightner, D. Nuclear Magnetic Resonance Biosensor for Rapid Detection of Vibrio Parahaemolyticus. *Biomed. J.* **2019**, *42* (3), 187−192.

(36) Lin, H.; Lu, Q.; Ge, S.; Cai, Q.; Grimes, C. A. Detection of Pathogen Escherichia Coli O157: H7 with a Wireless Magnetoelastic-Sensing Device Amplified by Using Chitosan-Modified Magnetic Fe3O4 Nanoparticles. *Sens. Actuators, B* **2010**, *147* (1), 343−349.

(37) Zou, D.; Jin, L.; Wu, B.; Hu, L.; Chen, X.; Huang, G.; Zhang, J. Rapid Detection of Salmonella in Milk by Biofunctionalised Magnetic Nanoparticle Cluster Sensor Based on Nuclear Magnetic Resonance. *Int. Dairy J.* **2019**, *91*, 82−88.

(38) Gao, Y.; Huo, W.; Zhang, L.; Lian, J.; Tao, W.; Song, C.; Tang, J.; Shi, S.; Gao, Y. Multiplex Measurement of Twelve Tumor Markers Using a GMR Multi-Biomarker Immunoassay Biosensor. *Biosens. Bioelectron.* **2019**, *123*, 204−210.

(39) Wang, T.; Yang, Z.; Lei, C.; Lei, J.; Zhou, Y. An Integrated Giant Magnetoimpedance Biosensor for Detection of Biomarker. *Biosens. Bioelectron.* **2014**, *58*, 338−344.

(40) Klein, T.; Wang, W.; Yu, L.; Wu, K.; Boylan, K. L.; Vogel, R. I.; Skubitz, A. P.; Wang, J.-P. Development of a Multiplexed Giant Magnetoresistive Biosensor Array Prototype to Quantify Ovarian Cancer Biomarkers. *Biosens. Bioelectron.* **2019**, *126*, 301−307.

(41) Wang, W.; Wang, Y.; Tu, L.; Klein, T.; Feng, Y.; Li, Q.; Wang, J.-P. Magnetic Detection of Mercuric Ion Using Giant Magnetoresistance-Based Biosensing System. *Anal. Chem.* **2014**, *86* (8), 3712−3716.

(42) Vidal, J. C.; Bertolín, J. R.; Bonel, L.; Asturias, L.; Arcos-Martínez, M. J.; Castillo, J. R. Rapid Determination of Recent Cocaine Use with Magnetic Particles-Based Enzyme Immunoassays in Serum, Saliva, and Urine Fluids. *J. Pharm. Biomed. Anal.* **2016**, *125*, 54−61.

(43) Krishna, V. D.; Wu, K.; Su, D.; Cheeran, M. C.; Wang, J.-P.; Perez, A. Nanotechnology: Review of Concepts and Potential Application of Sensing Platforms in Food Safety. *Food Microbiol.* **2018**, *75*, 47.

(44) Wu, K.; Su, D.; Saha, R.; Liu, J.; Chugh, V. K.; Wang, J.-P. Magnetic Particle Spectroscopy: A Short Review of Applications Using Magnetic Nanoparticles. *ACS Appl. Nano Mater.* **2020**.

(45) Pastucha, M.; Farka, Z.; Lacina, K.; Mikušová, Z.; Skládal, P. Magnetic Nanoparticles for Smart Electrochemical Immunoassays: A Review on Recent Developments. *Microchim. Acta* **2019**, *186* (5), 312.

(46) Schotter, J.; Kamp, P. B.; Becker, A.; Puhler, A.; Reiss, G.; Bruckl, H. Comparison of a Prototype Magnetoresistive Biosensor to Standard Fluorescent DNA Detection. *Biosens. Bioelectron.* **2004**, *19* (10), 1149−1156.

(47) Thomson, W. On the Electro-Dynamic Qualities of Metals:— Effects of Magnetization on the Electric Conductivity of Nickel and of Iron. *Proc. R. Soc. London* **1857**, No. 8, 546−550.

(48) McGuire, T.; Potter, R. L. Anisotropic Magnetoresistance in Ferromagnetic 3d Alloys. *IEEE Trans. Magn.* **1975**, *11* (4), 1018−1038.

(49) Fert, A.; Campbell, I. A. Electrical Resistivity of Ferromagnetic Nickel and Iron Based Alloys. *J. Phys. F: Met. Phys.* **1976**, *6* (5), 849.

(50) Baibich, M. N.; Broto, J. M.; Fert, A.; Van Dau, F. N.; Petroff, F.; Etienne, P.; Creuzet, G.; Friederich, A.; Chazelas, J. Giant Magnetoresistance of (001)Fe/(001)Cr Magnetic Superlattices. *Phys. Rev. Lett.* **1988**, *61* (21), 2472−2475.

(51) Binasch, G.; Grünberg, P.; Saurenbach, F.; Zinn, W. Enhanced Magnetoresistance in Layered Magnetic Structures with Antiferro-magnetic Interlayer Exchange. *Phys. Rev. B: Condens. Matter Mater. Phys.* **1989**, *39* (7), 4828−4830.

(52) Parkin, S.; Jiang, X.; Kaiser, C.; Panchula, A.; Roche, K.; Samant, M. Magnetically Engineered Spintronic Sensors and Memory. *Proc. IEEE* **2003**, *91* (5), 661−680.

(53) Bernardi, J.; Hütten, A.; Thomas, G. Electron Microscopy of Giant Magnetoresistive Granular Au— Co Alloys. *J. Magn. Magn. Mater.* **1996**, *157*, 153−155.

(54) Hütten, A.; Bernardi, J.; Friedrichs, S.; Thomas, G.; Balcells, L. Microstructural Influence on Magnetic Properties and Giant Magnetoresistance of Melt-Spun Gold-Cobalt. *Scr. Metall. Mater.* **1995**, *33* (10−11), 1647−1666.

(55) Garcia-Torres, J.; Vallés, E.; Gómez, E. Giant Magneto-resistance in Electrodeposited Co−Ag Granular Films. *Mater. Lett.* **2011**, *65* (12), 1865−1867.

(56) Kenane, S.; Voiron, J.; Benbrahim, N.; Chaînet, E.; Robaut, F. Magnetic Properties and Giant Magnetoresistance in Electrodeposited Co−Ag Granular Films. *J. Magn. Magn. Mater.* **2006**, *297* (2), 99−106.

(57) Odnodvorets, L. V.; Protsenko, I. Y.; Tkach, O. P.; Shabelnyk, Y. M.; Shumakova, N. I. Magnetoresistive Effect in Granular Film Alloys Based on Ag and Fe or Co. *J. Nano- Electron. Phys.* **2017**, *9* (2), 2021-1−2021-4.

(58) Melzer, M.; Karnaushenko, D.; Makarov, D.; Baraban, L.; Calvimontes, A.; Mönch, I.; Kaltofen, R.; Mei, Y.; Schmidt, O. G. Elastic Magnetic Sensor with Isotropic Sensitivity for In-Flow Detection of Magnetic Objects. *RSC Adv.* **2012**, *2* (6), 2284−2288.

(59) Melzer, M.; Karnaushenko, D.; Lin, G.; Baunack, S.; Makarov, D.; Schmidt, O. G. Direct Transfer of Magnetic Sensor Devices to Elastomeric Supports for Stretchable Electronics. *Adv. Mater.* **2015**, *27* (8), 1333−1338.

(60) Noh, E.-S.; Ulloa, S. E.; Lee, H.-M. A Theoretical Study of an Amorphous Aluminium Oxide Layer Used as a Tunnel Barrier in a Magnetic Tunnel Junction. *Phys. Status Solidi B* **2007**, *244* (12), 4427−4430.

(61) Gloos, K.; Koppinen, P. J.; Pekola, J. P. Properties of Native Ultrathin Aluminium Oxide Tunnel Barriers. *J. Phys.: Condens. Matter* **2003**, *15* (10), 1733.

(62) Parkin, S. S. P.; Kaiser, C.; Panchula, A.; Rice, P. M.; Hughes, B.; Samant, M.; Yang, S. H. Giant Tunnelling Magnetoresistance at Room Temperature with MgO (100) Tunnel Barriers. *Nat. Mater.* **2004**, *3* (12), 862−867.

(63) Yuasa, S.; Fukushima, A.; Nagahama, T.; Ando, K.; Suzuki, Y. High Tunnel Magnetoresistance at Room Temperature in Fully

Epitaxial Fe/MgO/Fe Tunnel Junctions Due to Coherent Spin-Polarized Tunneling. *Jpn. J. Appl. Phys.* **2004**, *43* (4B), L588.

(64) Ferreira, R.; Paz, E.; Freitas, P. P.; Wang, J.; Xue, S. Large Area and Low Aspect Ratio Linear Magnetic Tunnel Junctions with a Soft-Pinned Sensing Layer. *IEEE Trans. Magn.* **2012**, *48* (11), 3719−3722.

(65) Chen, J. Y.; Feng, J. F.; Coey, J. M. D. Tunable Linear Magnetoresistance in MgO Magnetic Tunnel Junction Sensors Using Two Pinned CoFeB Electrodes. *Appl. Phys. Lett.* **2012**, *100* (14), 142407.

(66) Cao, J.; Freitas, P. P. Wheatstone Bridge Sensor Composed of Linear MgO Magnetic Tunnel Junctions. *J. Appl. Phys.* **2010**, *107* (9), 09E712.

(67) Nowak, E. R.; Weissman, M. B.; Parkin, S. S. P. Electrical Noise in Hysteretic Ferromagnet−Insulator−Ferromagnet Tunnel Junctions. *Appl. Phys. Lett.* **1999**, *74* (4), 600−602.

(68) Wu, K.; Su, D.; Liu, J.; Saha, R.; Wang, J.-P. Magnetic Nanoparticles in Nanomedicine: A Review of Recent Advances. *Nanotechnology* **2019**, *30* (50), 502003.

(69) Moretti, D.; DiFrancesco, M. L.; Sharma, P. P.; Dante, S.; Albisetti, E.; Monticelli, M.; Bertacco, R.; Petti, D.; Baldelli, P.; Benfenati, F. Biocompatibility of a Magnetic Tunnel Junction Sensor Array for the Detection of Neuronal Signals in Culture. *Front. Neurosci.* **2018**, *12*, 909.

(70) Su, D.; Wu, K.; Saha, R.; Peng, C.; Wang, J.-P. Advances in Magnetoresistive Biosensors. *Micromachines* **2020**, *11* (1), 34.

(71) Baselt, D. R.; Lee, G. U.; Natesan, M.; Metzger, S. W.; Sheehan, P. E.; Colton, R. J. A Biosensor Based on Magnetoresistance Technology. *Biosens. Bioelectron.* **1998**, *13* (7), 731−739.

(72) Krishna, V. D.; Wu, K.; Perez, A. M.; Wang, J. P. Giant Magnetoresistance-Based Biosensor for Detection of Influenza A Virus. *Front. Microbiol.* **2016**, *7*, 8.

(73) Wu, K.; Klein, T.; Krishna, V. D.; Su, D.; Perez, A. M.; Wang, J.-P. Portable GMR Handheld Platform for the Detection of Influenza A Virus. *ACS Sens.* **2017**, *2*, 1594−1601.

(74) Choi, J.; Gani, A. W.; Bechstein, D. J.; Lee, J.-R.; Utz, P. J.; Wang, S. X. Portable, One-Step, and Rapid GMR Biosensor Platform with Smartphone Interface. *Biosens. Bioelectron.* **2016**, *85*, 1−7.

(75) Zhi, X.; Liu, Q. S.; Zhang, X.; Zhang, Y. X.; Feng, J.; Cui, D. X. Quick Genotyping Detection of HBV by Giant Magnetoresistive Biochip Combined with PCR and Line Probe Assay. *Lab Chip* **2012**, *12* (4), 741−745.

(76) Zhi, X.; Deng, M.; Yang, H.; Gao, G.; Wang, K.; Fu, H.; Zhang, Y.; Chen, D.; Cui, D. A Novel HBV Genotypes Detecting System Combined with Microfluidic Chip, Loop-Mediated Isothermal Amplification and GMR Sensors. *Biosens. Bioelectron.* **2014**, *54*, 372−377.

(77) Sun, X.; Lei, C.; Guo, L.; Zhou, Y. Separable Detecting of Escherichia Coli O157H: H7 by a Giant Magneto-Resistance-Based Bio-Sensing System. *Sens. Actuators, B* **2016**, *234*, 485−492.

(78) Gupta, S.; Kakkar, V. DARPin Based GMR Biosensor for the Detection of ESAT-6 Tuberculosis Protein. *Tuberculosis* **2019**, *118*, 101852.

(79) Grancharov, S. G.; Zeng, H.; Sun, S.; Wang, S. X.; O'Brien, S.; Murray, C.; Kirtley, J.; Held, G. Bio-Functionalization of Monodisperse Magnetic Nanoparticles and Their Use as Biomolecular Labels in a Magnetic Tunnel Junction Based Sensor. *J. Phys. Chem. B* **2005**, *109* (26), 13030−13035.

(80) Shen, W.; Schrag, B. D.; Carter, M. J.; Xiao, G. Quantitative Detection of DNA Labeled with Magnetic Nanoparticles Using Arrays of MgO-Based Magnetic Tunnel Junction Sensors. *Appl. Phys. Lett.* **2008**, *93* (3), 033903.

(81) Shen, W.; Schrag, B. D.; Carter, M. J.; Xie, J.; Xu, C.; Sun, S.; Xiao, G. Detection of DNA Labeled with Magnetic Nanoparticles Using MgO-Based Magnetic Tunnel Junction Sensors. *J. Appl. Phys.* **2008**, *103* (7), 7A306.

(82) Gervasoni, G.; Carminati, M.; Ferrari, G.; Sampietro, M.; Albisetti, E.; Petti, D.; Sharma, P.; Bertacco, R. A 12-Channel Dual-Lock-in Platform for Magneto-Resistive DNA Detection with Ppm

Resolution. *2014 IEEE Biomedical Circuits and Systems Conference (BioCAS) Proceedings*; IEEE, 2014; pp 316−319.

(83) Sharma, P. P.; Albisetti, E.; Massetti, M.; Scolari, M.; La Torre, C.; Monticelli, M.; Leone, M.; Damin, F.; Gervasoni, G.; Ferrari, G.; Salice, F.; Cerquaglia, E.; Falduti, G.; Cretich, M.; Marchisio, E.; Chiari, M.; Sampietro, M.; Petti, D.; Bertacco, R. Integrated Platform for Detecting Pathogenic DNA via Magnetic Tunneling Junction-Based Biosensors. *Sens. Actuators, B* **2017**, *242*, 280−287.

(84) Li, L.; Mak, K. Y.; Zhou, Y. Detection of HIV-1 Antigen Based on Magnetic Tunnel Junction Sensor and Magnetic Nanoparticles. *Chin. Phys. B* **2020**, *29*, 088701.

(85) Orlov, A. V.; Znoyko, S. L.; Cherkasov, V. R.; Nikitin, M. P.; Nikitin, P. I. Multiplex Biosensing Based on Highly Sensitive Magnetic Nanolabel Quantification: Rapid Detection of Botulinum Neurotoxins A, B, and E in Liquids. *Anal. Chem.* **2016**, *88* (21), 10419−10426.

(86) Orlov, A. V.; Khodakova, J. A.; Nikitin, M. P.; Shepelyakovskaya, A. O.; Brovko, F. A.; Laman, A. G.; Grishin, E. V.; Nikitin, P. I. Magnetic Immunoassay for Detection of Staphylococcal Toxins in Complex Media. *Anal. Chem.* **2013**, *85*, 1154−1163.

(87) Wu, K.; Liu, J.; Saha, R.; Su, D.; Krishna, V. D.; Cheeran, M. C.-J.; Wang, J.-P. Magnetic Particle Spectroscopy for Detection of Influenza A Virus Subtype H1N1. *ACS Appl. Mater. Interfaces* **2020**, *12* (12), 13686−13697.

(88) Pietschmann, J.; Voepel, N.; Spiegel, H.; Krause, H.-J.; Schroeper, F. Brief Communication: Magnetic Immuno-Detection of SARS-CoV-2 Specific Antibodies. *bioRxiv* **2020**.

(89) Luo, Y.; Alocilja, E. C. Portable Nuclear Magnetic Resonance Biosensor and Assay for a Highly Sensitive and Rapid Detection of Foodborne Bacteria in Complex Matrices. *J. Biol. Eng.* **2017**, *11* (1), 14.

(90) Liong, M.; Hoang, A. N.; Chung, J.; Gural, N.; Ford, C. B.; Min, C.; Shah, R. R.; Ahmad, R.; Fernandez-Suarez, M.; Fortune, S. M.; Toner, M.; Lee, H.; Weissleder, R. Magnetic Barcode Assay for Genetic Detection of Pathogens. *Nat. Commun.* **2013**, *4* (1), 1−9.

(91) Nikitin, P. I.; Vetoshko, P. M.; Ksenevich, T. I. New Type of Biosensor Based on Magnetic Nanoparticle Detection. *J. Magn. Magn. Mater.* **2007**, *311*, 445−449.

(92) Krause, H.-J.; Wolters, N.; Zhang, Y.; Offenhäusser, A.; Miethe, P.; Meyer, M. H.; Hartmann, M.; Keusgen, M. Magnetic Particle Detection by Frequency Mixing for Immunoassay Applications. *J. Magn. Magn. Mater.* **2007**, *311*, 436−444.

(93) Gleich, B.; Weizenecker, J. Tomographic Imaging Using the Nonlinear Response of Magnetic Particles. *Nature* **2005**, *435* (7046), 1214−1217.

(94) Wu, K.; Su, D.; Saha, R.; Wong, D.; Wang, J.-P. Magnetic Particle Spectroscopy-Based Bioassays: Methods, Applications, Advances, and Future Opportunities. *J. Phys. D: Appl. Phys.* **2019**, *52*, 173001.

(95) Zhang, X.; Reeves, D. B.; Perreard, I. M.; Kett, W. C.; Griswold, K. E.; Gimi, B.; Weaver, J. B. Molecular Sensing with Magnetic Nanoparticles Using Magnetic Spectroscopy of Nanoparticle Brownian Motion. *Biosens. Bioelectron.* **2013**, *50*, 441−446.

(96) Khurshid, H.; Shi, Y.; Berwin, B. L.; Weaver, J. B. Evaluating Blood Clot Progression Using Magnetic Particle Spectroscopy. *Med. Phys.* **2018**, *45* (7), 3258−3263.

(97) Znoyko, S. L.; Orlov, A. V.; Bragina, V. A.; Nikitin, M. P.; Nikitin, P. I. Nanomagnetic Lateral Flow Assay for High-Precision Quantification of Diagnostically Relevant Concentrations of Serum TSH. *Talanta* **2020**, *216*, 120961.

(98) Znoyko, S. L.; Orlov, A. V.; Pushkarev, A. V.; Mochalova, E. N.; Guteneva, N. V.; Lunin, A. V.; Nikitin, M. P.; Nikitin, P. I. Ultrasensitive Quantitative Detection of Small Molecules with Rapid Lateral-Flow Assay Based on High-Affinity Bifunctional Ligand and Magnetic Nanolabels. *Anal. Chim. Acta* **2018**, *1034*, 161−167.

(99) Wu, K.; Liu, J.; Su, D.; Saha, R.; Wang, J.-P. Magnetic Nanoparticle Relaxation Dynamics-Based Magnetic Particle Spectros-

copy for Rapid and Wash-Free Molecular Sensing. *ACS Appl. Mater. Interfaces* **2019**, *11* (26), 22979−22986.

(100) Wu, K.; Schliep, K.; Zhang, X.; Liu, J.; Ma, B.; Wang, J. Characterizing Physical Properties of Superparamagnetic Nanoparticles in Liquid Phase Using Brownian Relaxation. *Small* **2017**, *13*, 1604135.

(101) Wu, K.; Batra, A.; Jain, S.; Wang, J.-P. Magnetization Response Spectroscopy of Superparamagnetic Nanoparticles Under Mixing Frequency Fields. *IEEE Trans. Magn.* **2016**, *52*, 1−4.

(102) Shi, Y.; Jyoti, D.; Gordon-Wylie, S. W.; Weaver, J. B. Quantification of Magnetic Nanoparticles by Compensating for Multiple Environment Changes Simultaneously. *Nanoscale* **2020**, *12* (1), 195−200.

(103) Bragina, V. A.; Znoyko, S. L.; Orlov, A. V.; Pushkarev, A. V.; Nikitin, M. P.; Nikitin, P. I. Analytical Platform with Selectable Assay Parameters Based on Three Functions of Magnetic Nanoparticles: Demonstration of Highly Sensitive Rapid Quantitation of Staphylococcal Enterotoxin B in Food. *Anal. Chem.* **2019**, *91* (15), 9852−9857.

(104) Guteneva, N. V.; Znoyko, S. L.; Orlov, A. V.; Nikitin, M. P.; Nikitin, P. I. Rapid Lateral Flow Assays Based on the Quantification of Magnetic Nanoparticle Labels for Multiplexed Immunodetection of Small Molecules: Application to the Determination of Drugs of Abuse. *Microchim. Acta* **2019**, *186* (9), 621.

(105) Wu, K.; Tu, L.; Su, D.; Wang, J.-P. Magnetic Dynamics of Ferrofluids: Mathematical Models and Experimental Investigations. *J. Phys. D: Appl. Phys.* **2017**, *50* (8), 085005.

(106) Wu, K.; Su, D.; Saha, R.; Liu, J.; Wang, J.-P. Investigating the Effect of Magnetic Dipole−Dipole Interaction on Magnetic Particle Spectroscopy: Implications for Magnetic Nanoparticle-Based Bioassays and Magnetic Particle Imaging. *J. Phys. D: Appl. Phys.* **2019**, *52* (33), 335002.

(107) Draack, S.; Viereck, T.; Kuhlmann, C.; Schilling, M.; Ludwig, F. Temperature-Dependent MPS Measurements. *Int. J. Magn. Part. Imaging* **2017**, *3* (1).

(108) Perreard, I.; Reeves, D.; Zhang, X.; Kuehlert, E.; Forauer, E.; Weaver, J. Temperature of the Magnetic Nanoparticle Microenvironment: Estimation from Relaxation Times. *Phys. Med. Biol.* **2014**, *59*, 1109.

(109) Wu, K.; Liu, J.; Wang, Y.; Ye, C.; Feng, Y.; Wang, J.-P. Superparamagnetic Nanoparticle-Based Viscosity Test. *Appl. Phys. Lett.* **2015**, *107*, 053701.

(110) Utkur, M.; Muslu, Y.; Saritas, E. U. Relaxation-Based Viscosity Mapping for Magnetic Particle Imaging. *Phys. Med. Biol.* **2017**, *62* (9), 3422.

(111) Liu, J.; Su, D.; Wu, K.; Wang, J.-P. High-Moment Magnetic Nanoparticles. *J. Nanopart. Res.* **2020**, *22* (3), 1−16.

(112) Anfossi, L.; Di Nardo, F.; Russo, A.; Cavalera, S.; Giovannoli, C.; Spano, G.; Baumgartner, S.; Lauter, K.; Baggiani, C. Silver and Gold Nanoparticles as Multi-Chromatic Lateral Flow Assay Probes for the Detection of Food Allergens. *Anal. Bioanal. Chem.* **2019**, *411* (9), 1905−1913.

(113) Ruppert, C.; Phogat, N.; Laufer, S.; Kohl, M.; Deigner, H.-P. A Smartphone Readout System for Gold Nanoparticle-Based Lateral Flow Assays: Application to Monitoring of Digoxigenin. *Microchim. Acta* **2019**, *186* (2), 119.

(114) Wang, C.; Xiao, R.; Wang, S.; Yang, X.; Bai, Z.; Li, X.; Rong, Z.; Shen, B.; Wang, S. Magnetic Quantum Dot Based Lateral Flow Assay Biosensor for Multiplex and Sensitive Detection of Protein Toxins in Food Samples. *Biosens. Bioelectron.* **2019**, *146*, 111754.

(115) Wang, J.; Meng, H.-M.; Chen, J.; Liu, J.; Zhang, L.; Qu, L.; Li, Z.; Lin, Y. Quantum Dot-Based Lateral Flow Test Strips for Highly Sensitive Detection of the Tetanus Antibody. *ACS Omega* **2019**, *4* (4), 6789−6795.

(116) Zhu, M.; Jia, Y.; Peng, L.; Ma, J.; Li, X.; Shi, F. A Highly Sensitive Dual-Color Lateral Flow Immunoassay for Brucellosis Using One-Step Synthesized Latex Microspheres. *Anal. Methods* **2019**, *11* (22), 2937−2942.

(117) Shultz, M. D.; Calvin, S.; Fatouros, P. P.; Morrison, S. A.; Carpenter, E. E. Enhanced Ferrite Nanoparticles as MRI Contrast Agents. *J. Magn. Magn. Mater.* **2007**, *311* (1), 464−468.

(118) Dash, A.; Blasiak, B.; Tomanek, B.; van Veggel, F. C. Validation of Inner, Second, and Outer Sphere Contributions to T1 and T2 Relaxation in Gd3+-Based Nanoparticles Using Eu3+ Lifetime Decay as a Probe. *J. Phys. Chem. C* **2018**, *122* (21), 11557−11569.

(119) Bonnet, C. S.; Fries, P. H.; Crouzy, S.; Delangle, P. Outer-Sphere Investigation of MRI Relaxation Contrast Agents. Example of a Cyclodecapeptide Gadolinium Complex with Second-Sphere Water. *J. Phys. Chem. B* **2010**, *114* (26), 8770−8781.

(120) Dupré, A.; Lei, K.-M.; Mak, P.-I.; Martins, R. P.; Peng, W. K. Micro-and Nanofabrication NMR Technologies for Point-of-Care Medical Applications−A Review. *Microelectron. Eng.* **2019**, *209*, 66−74.

(121) Zalesskiy, S. S.; Danieli, E.; Blümich, B.; Ananikov, V. P. Miniaturization of NMR Systems: Desktop Spectrometers, Microcoil Spectroscopy, and "NMR on a Chip" for Chemistry, Biochemistry, and Industry. *Chem. Rev.* **2014**, *114* (11), 5641−5694.

(122) Weissleder, R.; Lee, H.; Ham, D.; Sun, N.; Liu, Y. Miniaturized Magnetic Resonance Systems and Methods. Google Patent, 2011.

(123) Bemetz, J.; Wegemann, A.; Saatchi, K.; Haase, A.; Häfeli, U. O.; Niessner, R.; Gleich, B.; Seidel, M. Microfluidic-Based Synthesis of Magnetic Nanoparticles Coupled with Miniaturized NMR for Online Relaxation Studies. *Anal. Chem.* **2018**, *90* (16), 9975−9982.

(124) Lee, H.; Sun, E.; Ham, D.; Weissleder, R. Chip−NMR Biosensor for Detection and Molecular Analysis of Cells. *Nat. Med.* **2008**, *14* (8), 869.

(125) Castro, C. M.; Ghazani, A. A.; Chung, J.; Shao, H.; Issadore, D.; Yoon, T.-J.; Weissleder, R.; Lee, H. Miniaturized Nuclear Magnetic Resonance Platform for Detection and Profiling of Circulating Tumor Cells. *Lab Chip* **2014**, *14* (1), 14−23.

(126) Korvink, J. G.; MacKinnon, N.; Badilita, V.; Jouda, M. Small Is Beautiful" in NMR. *J. Magn. Reson.* **2019**, *306*, 112−117.

(127) Causier, A.; Carret, G.; Boutin, C.; Berthelot, T.; Berthault, P. 3D-Printed System Optimizing Dissolution of Hyperpolarized Gaseous Species for Micro-Sized NMR. *Lab Chip* **2015**, *15* (9), 2049−2054.

(128) Kalfe, A.; Telfah, A.; Lambert, J.; Hergenröder, R. Looking into Living Cell Systems: Planar Waveguide Microfluidic NMR Detector for in Vitro Metabolomics of Tumor Spheroids. *Anal. Chem.* **2015**, *87* (14), 7402−7410.

(129) Liu, Y.; Sun, N.; Lee, H.; Weissleder, R.; Ham, D. CMOS Mini Nuclear Magnetic Resonance System and Its Application for Biomolecular Sensing. *2008 IEEE International Solid-State Circuits Conference-Digest of Technical Papers*; IEEE, 2008; pp 140−602.

(130) Blümich, B. Introduction to Compact NMR: A Review of Methods. *TrAC, Trends Anal. Chem.* **2016**, *83*, 2−11.

(131) Brand, O.; Fedder, G. K.; Hierold, C.; Tabata, O. *Micro and Nano Scale NMR: Technologies and Systems*; John Wiley & Sons, 2018.

(132) Lei, K.-M.; Mak, P.-I.; Law, M.-K.; Martins, R. P. *Handheld Total Chemical and Biological Analysis Systems*; Springer, 2018.

(133) Lei, K.-M.; Sun, N.; Mak, P.-I.; Martins, R. P.; Ham, D. Micro-NMR on CMOS for Biomolecular Sensing. *CMOS Circuits for Biological Sensing and Processing*; Springer, 2018; pp 101−132.

(134) Issadore, D.; Min, C.; Liong, M.; Chung, J.; Weissleder, R.; Lee, H. Miniature Magnetic Resonance System for Point-of-Care Diagnostics. *Lab Chip* **2011**, *11* (13), 2282−2287.

(135) Viegas, A.; Manso, J.; Nobrega, F. L.; Cabrita, E. J. Saturation-Transfer Difference (STD) NMR: A Simple and Fast Method for Ligand Screening and Characterization of Protein Binding. *J. Chem. Educ.* **2011**, *88* (7), 990−994.

(136) Yue, D.; Zhang, Y.; Cheng, L.; Ma, J.; Xi, Y.; Yang, L.; Su, C.; Shao, B.; Huang, A.; Xiang, R.; Cheng, P. Hepatitis B Virus X Protein (HBx)-Induced Abnormalities of Nucleic Acid Metabolism Revealed by 1 H-NMR-Based Metabonomics. *Sci. Rep.* **2016**, *6* (1), 1−13.

(137) Kusunoki, H.; Tanaka, T.; Kohno, T.; Kimura, H.; Hosoda, K.; Wakamatsu, K.; Hamaguchi, I. NMR Characterization of the

Interaction between Bcl-XL and the BH3-like Motif of Hepatitis B Virus X Protein. *Biochem. Biophys. Res. Commun.* **2019**, *518* (3), 445−450.

(138) Dapiaggi, F.; Pieraccini, S.; Potenza, D.; Vasile, F.; Macut, H.; Pellegrino, S.; Aliverti, A.; Sironi, M. Computer Aided Design and NMR Characterization of an Oligopeptide Targeting the Ebola Virus VP24 Protein. *New J. Chem.* **2017**, *41* (11), 4308−4315.

(139) Vasile, F.; Gubinelli, F.; Panigada, M.; Soprana, E.; Siccardi, A.; Potenza, D. NMR Interaction Studies of Neu5Ac-α-(2, 6)-Gal-β-(1−4)-GlcNAc with Influenza-Virus Hemagglutinin Expressed in Transfected Human Cells. *Glycobiology* **2018**, *28* (1), 42−49.

(140) Weaver, J. B.; Shi, Y.; Ness, D. B.; Khurshid, H.; Samia, A. C. S. Sensitivity Limits for in Vivo Elisa Measurements of Molecular Biomarker Concentrations. *Int. J. Magn. Part. Imaging* **2017**, *3* (2).

(141) Guedes, A.; Almeida, J. M.; Cardoso, S.; Ferreira, R.; Freitas, P. P. Improving Magnetic Field Detection Limits of Spin Valve Sensors Using Magnetic Flux Guide Concentrators. *IEEE Trans. Magn.* **2007**, *43* (6), 2376−2378.

(142) Lee, K.; Lee, S.; Cho, B. K.; Kim, K.-S.; Kim, B. The Limit of Detection of Giant Magnetoresistive (GMR) Sensors for Bio-Applications. *J. Korean Phys. Soc.* **2009**, *55* (1), 193−196.

(143) Paysen, H.; Wells, J.; Kosch, O.; Steinhoff, U.; Franke, J.; Trahms, L.; Schaeffter, T.; Wiekhorst, F. Improved Sensitivity and Limit-of-Detection Using a Receive-Only Coil in Magnetic Particle Imaging. *Phys. Med. Biol.* **2018**, *63* (13), 13NT02.

(144) Griffiths, L. Assay by Nuclear Magnetic Resonance Spectroscopy: Quantification Limits. *Analyst* **1998**, *123* (5), 1061−1068.

(145) Mompeán, M.; Sánchez-Donoso, R. M.; De La Hoz, A.; Saggiomo, V.; Velders, A. H.; Gomez, M. V. Pushing Nuclear Magnetic Resonance Sensitivity Limits with Microfluidics and Photo-Chemically Induced Dynamic Nuclear Polarization. *Nat. Commun.* **2018**, *9* (1), 1−8.

(146) Wang, S. X.; Li, G. Advances in Giant Magnetoresistance Biosensors with Magnetic Nanoparticle Tags: Review and Outlook. *IEEE Trans. Magn.* **2008**, *44* (7), 1687−1702.

(147) Chou, T.-C.; Hsu, W.; Wang, C.-H.; Chen, Y.-J.; Fang, J.-M. Rapid and Specific Influenza Virus Detection by Functionalized Magnetic Nanoparticles and Mass Spectrometry. *J. Nanobiotechnol.* **2011**, *9* (1), 52.

(148) Tian, B.; Liao, X.; Svedlindh, P.; Strömberg, M.; Wetterskog, E. Ferromagnetic Resonance Biosensor for Homogeneous and Volumetric Detection of DNA. *ACS Sens.* **2018**, *3* (6), 1093−1101.

(149) Barrios-Gumiel, A.; Sepúlveda-Crespo, D.; Jiménez, J. L.; Gómez, R.; Muñoz-Fernández, M. Á.; de la Mata, F. J. Dendronized Magnetic Nanoparticles for HIV-1 Capture and Rapid Diagnostic. *Colloids Surf., B* **2019**, *181*, 360−368.

(150) Zhang, F.; Luo, L.; Gong, H.; Chen, C.; Cai, C. A Magnetic Molecularly Imprinted Optical Chemical Sensor for Specific Recognition of Trace Quantities of Virus. *RSC Adv.* **2018**, *8* (56), 32262−32268.

(151) Luo, L.; Yang, J.; Liang, K.; Chen, C.; Chen, X.; Cai, C. Fast and Sensitive Detection of Japanese Encephalitis Virus Based on a Magnetic Molecular Imprinted Polymer−Resonance Light Scattering Sensor. *Talanta* **2019**, *202*, 21−26.

(152) Sun, Y.; Xu, L.; Zhang, F.; Song, Z.; Hu, Y.; Ji, Y.; Shen, J.; Li, B.; Lu, H.; Yang, H. A Promising Magnetic SERS Immunosensor for Sensitive Detection of Avian Influenza Virus. *Biosens. Bioelectron.* **2017**, *89*, 906−912.

(153) Wang, G.; Gao, Y.; Huang, H.; Su, X. Multiplex Immunoassays of Equine Virus Based on Fluorescent Encoded Magnetic Composite Nanoparticles. *Anal. Bioanal. Chem.* **2010**, *398* (2), 805−813.

(154) Ali, Z.; Wang, J.; Tang, Y.; Liu, B.; He, N.; Li, Z. Simultaneous Detection of Multiple Viruses Based on Chemiluminescence and Magnetic Separation. *Biomater. Sci.* **2017**, *5* (1), 57−66.

(155) Zong, C.; Fang, L.; Song, F.; Wang, A.; Wan, Y. Fluorescent Fingerprint Bacteria by Multi-Channel Magnetic Fluorescent Nanosensor. *Sens. Actuators, B* **2019**, *289*, 234−241.

(156) Kim, D.; Lee, Y.-D.; Jo, S.; Kim, S.; Lee, T. S. Detection and Imaging of Cathepsin L in Cancer Cells Using the Aggregation of Conjugated Polymer Dots and Magnetic Nanoparticles. *Sens. Actuators, B* **2020**, *307*, 127641.

(157) Man, Y.; Jin, X.; Fu, H.; Pan, L. A Magnetic Nanoparticle Based Immunoassay for Alternariol Monomethyl Ether Using Hydrogen Peroxide-Mediated Fluorescence Quenching of CdTe Quantum Dots. *Microchim. Acta* **2019**, *186* (4), 221.

(158) Zheng, X.; Zhao, L.; Wen, D.; Wang, X.; Yang, H.; Feng, W.; Kong, J. Ultrasensitive Fluorescent Detection of HTLV-II DNA Based on Magnetic Nanoparticles and Atom Transfer Radical Polymerization Signal Amplification. *Talanta* **2020**, *207*, 120290.

(159) Metaxas, P. J.; Sushruth, M.; Begley, R. A.; Ding, J.; Woodward, R. C.; Maksymov, I. S.; Albert, M.; Wang, W.; Fangohr, H.; Adeyeye, A. O.; Kostylev, M. Sensing Magnetic Nanoparticles Using Nano-Confined Ferromagnetic Resonances in a Magnonic Crystal. *Appl. Phys. Lett.* **2015**, *106* (23), 232406.

(160) Sushruth, M.; Ding, J.; Duczynski, J.; Woodward, R. C.; Begley, R. A.; Fangohr, H.; Fuller, R. O.; Adeyeye, A. O.; Kostylev, M.; Metaxas, P. J. Resonance-Based Detection of Magnetic Nanoparticles and Microbeads Using Nanopatterned Ferromagnets. *Phys. Rev. Appl.* **2016**, *6* (4), 044005.

(161) Albert, M.; Beg, M.; Chernyshenko, D.; Bisotti, M.-A.; Carey, R. L.; Fangohr, H.; Metaxas, P. J. Frequency-Based Nanoparticle Sensing over Large Field Ranges Using the Ferromagnetic Resonances of a Magnetic Nanodisc. *Nanotechnology* **2016**, *27* (45), 455502.

(162) Saha, R.; Wu, K.; Su, D.; Wang, J.-P. Spin Current Nano-Oscillator (SCNO) as a Potential Frequency-Based, Ultra-Sensitive Magnetic Biosensor: A Simulation Study. *Nanotechnology* **2020**, *31*, 375501.

(163) Bai, Z.; Liu, Y.; Kong, R.; Nie, T.; Sun, Y.; Li, H.; Sun, T.; Pandey, C.; Wang, Y.; Zhang, H. Near-Field Terahertz Sensing of Hela Cells and Pseudomonas Based on Monolithic Integrated Metamaterials with Spintronic Terahertz Emitter. *ACS Appl. Mater. Interfaces* **2020**, *12*, 35895.

(164) Li, Y.; Xia, L. Coronavirus Disease 2019 (COVID-19): Role of Chest CT in Diagnosis and Management. *AJR, Am. J. Roentgenol.* **2020**, *214* (6), 1280−1286.

(165) Guo, L.; Ren, L.; Yang, S.; Xiao, M.; Chang, D.; Yang, F.; Dela Cruz, C. S.; Wang, Y.; Wu, C.; Xiao, Y. Profiling Early Humoral Response to Diagnose Novel Coronavirus Disease (COVID-19). *Clin. Infect. Dis.* **2020**, *71*, 778.

(166) Chan, J. F.-W.; Yip, C. C.-Y.; To, K. K.-W.; Tang, T. H.-C.; Wong, S. C.-Y.; Leung, K.-H.; Fung, A. Y.-F.; Ng, A. C.-K.; Zou, Z.; Tsoi, H.-W.et al. Improved Molecular Diagnosis of COVID-19 by the Novel, Highly Sensitive and Specific COVID-19-RdRp/Hel Real-Time Reverse Transcription-PCR Assay Validated in Vitro and with Clinical Specimens. *J. Clin. Microbiol.* **2020**, *58* (5). DOI: 10.1128/JCM.00310-20

(167) Zhai, P.; Ding, Y.; Wu, X.; Long, J.; Zhong, Y.; Li, Y. The Epidemiology, Diagnosis and Treatment of COVID-19. *Int. J. Antimicrob. Agents* **2020**, *55*, 105955.

(168) Long, C.; Xu, H.; Shen, Q.; Zhang, X.; Fan, B.; Wang, C.; Zeng, B.; Li, Z.; Li, X.; Li, H. Diagnosis of the Coronavirus Disease (COVID-19): RRT-PCR or CT? *Eur. J. Radiol.* **2020**, *126*, 108961.

(169) Denmark, D. J.; Bustos-Perez, X.; Swain, A.; Phan, M.-H.; Mohapatra, S.; Mohapatra, S. S. Readiness of Magnetic Nanobiosensors for Point-of-Care Commercialization. *J. Electron. Mater.* **2019**, *48* (8), 4749−4761.

(170) Nabaei, V.; Chandrawati, R.; Heidari, H. Magnetic Biosensors: Modelling and Simulation. *Biosens. Bioelectron.* **2018**, *103*, 69−86.

(171) Udugama, B.; Kadhiresan, P.; Kozlowski, H. N.; Malekjahani, A.; Osborne, M.; Li, V. Y.; Chen, H.; Mubareka, S.; Gubbay, J. B.; Chan, W. C. Diagnosing COVID-19: The Disease and Tools for Detection. *ACS Nano* **2020**, *14* (4), 3822−3835.